APL Materials

Black silicon for near-infrared and ultraviolet photodetection: A review

Cite as: APL Mater. **11**, 021107 (2023); https://doi.org/10.1063/5.0133770
Submitted: 14 November 2022 • Accepted: 17 January 2023 • Published Online: 13 February 2023

Zhou Zhao, Zengxing Zhang, Junmin Jing, et al.

Submit Today!
APL Materials
Special Topic: Materials Challenges for Catalysis

© 2023 Author(s).

Black silicon for near-infrared and ultraviolet photodetection: A review

Cite as: APL Mater. 11, 021107 (2023); doi: 10.1063/5.0133770
Submitted: 14 November 2022 • Accepted: 17 January 2023 •
Published Online: 13 February 2023

Zhou Zhao,[1] Zengxing Zhang,[2,a)] Junmin Jing,[1] Rui Gao,[1] Zhiwei Liao,[1] Wenjun Zhang,[2] Guohua Liu,[3] Yonghua Wang,[1] Kaiying Wang,[4] and Chenyang Xue[1]

AFFILIATIONS

[1] Key Laboratory of Instrumentation Science and Dynamic Measurement, Ministry of Education, North University of China, Taiyuan 030051, China
[2] School of Aerospace Engineering, Xiamen University, Xiamen 361102, China
[3] Beijing Key Laboratory of Multiphase Flow and Heat Transfer for Low Grade Energy Utilization, North China Electric Power University, Beijing 102206, China
[4] Department of Microsystems, University of South-Eastern Norway, 3184 Horten, Norway

[a)] **Author to whom correspondence should be addressed:** zhangzengxing@xmu.edu.cn

ABSTRACT

As a typical representative of micro/nano-textured silicon, black silicon has excellent light absorption properties and is gradually surfacing as a substitute for standard silicon in photoelectric devices. Black silicon overcomes the limitations of traditional silicon-based devices, which are unable to achieve infrared light detection at wavelengths >1100 nm and have low quantum efficiency and sensitivity in ultraviolet light detection. In this article, the recent theoretical and experimental breakthroughs in near-infrared and ultraviolet detection using black silicon are summarized in detail. First, black silicon and the techniques for its fabrication are introduced. Then, the application of enhanced black silicon photodetectors within or above the bandgap limit and black silicon fabricated using different methods in infrared detection is discussed. In principle, infrared detection using black silicon is achieved by jointly utilizing element doping, localized surface plasmon resonance effect, and heterojunction formation. In addition, the application of black silicon in ultraviolet detection is also introduced. Ultraviolet detection is realized by an induced junction and the self-built electric field between black silicon and aluminum oxide. Finally, the increasingly growing potential of black silicon in near-infrared and ultraviolet detection applications, such as infrared night vision imaging, signal detection, ultraviolet light intensity monitoring, and national defense early warning, is further discussed.

© 2023 Author(s). All article content, except where otherwise noted, is licensed under a Creative Commons Attribution (CC BY) license (http://creativecommons.org/licenses/by/4.0/). https://doi.org/10.1063/5.0133770

I. INTRODUCTION

Black silicon is a silicon material with micro- and nanoscale structures exhibiting holes, needles, and pillar structures on the wafer surface. The first time black silicon was discovered and reported was by Jansen *et al.*[1] at the University of Twente in 1995, and the method to produce it is based on plasma etching. Then, in 1998, the team of Her *et al.*[2] of Harvard University who irradiated silicon with 500 femtosecond (fs) laser pulses in SF_6 and observed the formation of sharp cone-shaped spikes and arrays of silicon nanoparticles on the silicon surface is the first to highlight the potential of black silicon regarding its promising optical properties. The resulting material is black and covered with micro/nano-spikes and was named black silicon. The bandgap of conventional silicon is 1.12 eV, which limits its useful wavelength range to wavelengths smaller than 1.1 μm. Moreover, the light absorption ability is extremely low. Black silicon fabricated by femtosecond laser irradiation can effectively improve this problem. In the femtosecond laser method, the silicon surface is etched by a femtosecond laser with ultra-intensive pulse energy. First, SF_6 gas on the silicon surface is irradiated by a high-energy laser, causing ionization and decomposition and ultrafast melting and ultrafast condensation on the silicon surface. During irradiation, vaporized silicon atoms are formed on the surface, and S atoms that are generated by the decomposition of SF_6 bind to the silicon surface, resulting in hyperdoping of black silicon. SF_6 decomposes to

© Author(s) 2023

produce F^- ions and reacts with the vaporized silicon atoms to generate volatile gases, such as SiF_2 and SiF_4, which promote the etching of the silicon surface. Multiple irradiations with the femtosecond laser result in the formation of a sharp cone array of the doped microstructure with a certain height on the silicon surface. Black silicon fabricated by the femtosecond laser induces the formation of a microstructured cone array with a light-trapping effect on the surface of crystalline silicon, which achieves ultra-low light reflection. The energy band structure of single crystal silicon is changed to enable the absorption of photon energy below the forbidden bandwidth, and light absorption in the range of 1100–2500 nm exceeds 90%.[3] Due to its high absorption in the visible and infrared (IR) wavelength range, black silicon can be used in photodetectors, night vision cameras, and near-infrared (near-IR) avalanche photodiodes (APDs). Recent studies have found that when aluminum oxide is used as a passivation layer, it will also form an induced junction and a self-built electric field with the black silicon substrate to achieve an external quantum efficiency (EQE) of 96%[4] in the ultraviolet spectral range, which can be used in astronomy, missile warning, pollution monitoring, ultraviolet communication, etc. Therefore, due to its excellent optical properties, black silicon has great prospects in the application of the near-infrared and ultraviolet sensing technology, which is a promising technology for the manufacturing of high-performance silicon-based detectors.

This article reviews the recent progress of black silicon applications in the near-infrared and ultraviolet detection technology. The enhanced infrared photodetectors can be divided into photodetectors within or above the bandgap limit. For the former, black silicon as the substrate is mainly fabricated by metal-assisted chemical etching (MACE) and reactive ion etching (RIE), while for the latter, black silicon is mostly fabricated by femto- and nanosecond laser methods. As part of studies, only the substrate of black silicon has been fabricated. Although the photodetector is not obtained directly, black silicon has shown great potential for the application in infrared photodetectors. By applying the Localized Surface Plasmon Resonance (LSPR) effect, passivation layers (SiO_2, Al_2O_3, C_3N_4, etc.), and heterojunctions to black silicon, higher-performance black silicon is obtained for infrared photodetectors, which are used for infrared pixel arrays, room temperature infrared signal detection, security monitoring, etc. A novel type of black silicon based PIN photodetector with atomic layer deposition (ALD)-deposited alumina provides a good reference for ultraviolet detection. The future application prospects of black silicon near-infrared and ultraviolet photodetection are discussed and summarized.

II. FABRICATION

Since its discovery, black silicon has gradually become a substitute for silicon in silicon-based devices due to its excellent light absorption.[5] Infrared detection technology of black silicon has also become a research hotspot. The fabrication of black silicon based infrared detectors can be mainly improved by two aspects: 1. Structure of black silicon: fabrication of black silicon with uniform morphology and high light absorption. 2. Modification of physical properties (addition of auxiliary materials): LSPR, anti-reflection films (SiO_2,[6] Al_2O_3,[7,8] and C_3N_4[9]), hyper-doping, heterojunction, etc. Typical fabrication methods for black silicon with different structures include femtosecond laser,[10] nanosecond laser,[11] reactive ion etching,[12–14] plasma immersion ion implantation (PIII) etching,[15,16] and metal-assisted chemical etching.[7,17] The main progress of these methods is shown in Fig. 1.[1,2,15,18–31]

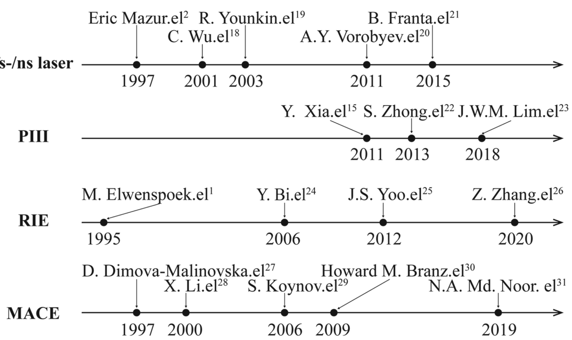

FIG. 1. The main progress of black silicon fabricated by different methods.

A. Femto/nanosecond laser irradiation

Femtosecond lasers use a powerful pulse with high energy in SF_6 atmosphere to scan the surface of the silicon wafer. The high-energy laser not only ionizes and decomposes SF_6 but also evaporates silicon at its solid surface. The generated S atoms are bound to the silicon surface, resulting in supersaturated doping. F^- atoms react with the vaporized silicon atoms to produce compounds such as SiF_2 and SiF_4 and promote melting and condensation of the silicon surface. Finally, multiple femtosecond laser pulses were applied to achieve a certain height of the doped microstructured cone array on the silicon surface. However, laser irradiation will damage the black silicon surface, and post-annealing treatment is often used to repair the damage of structural defects.[32]

The femtosecond laser can form an intermediate band in silicon due to sulfur doping, which is the impurity energy level. With this strategy, electrons are excited easier to make transitions at lower energies. Thus, the absorption in the near-infrared spectrum is greatly enhanced. Black silicon materials show near-unity absorption in the near-infrared spectral range owing to sulfur (S) hyperdoping and texturing of the Si surface.[33]

B. Plasma immersion ion implantation etching

PIII etching is a surface modification technique that utilizes high-voltage pulsed DC or pure DC power to implant accelerated ions into a suitable substrate.[5] The principle of PIII etching is that SF_6 and O_2 are ionized under the injection power to generate $SF_X{}^+$, F^*, and O^*. The $SF_X{}^+$ and F^* groups react with Si and generate the volatile gas SiF_4, which etches the silicon wafer. At the same time, the O^* and F^* groups combine with Si to form non-volatile $Si_xO_yF_z$, which prevents the formation of SiF_4 and passivates the surface. In addition, the accelerated plasma bombardment of the surface will decompose $Si_xO_yF_z$, balancing the etching effect mentioned above and surface passivation. In summary, plasma immersion ion implantation is accomplished by etching, passivation, and bombardment of the surface by high-energy ions.

© Author(s) 2023

In particular, a method called cryogenic plasma etching that is quite similar to the PIII but the main point is that it is performed at cryogenic temperatures belongs to PIII.[34] Black silicon fabricated only by PIII etching does not exhibit enhanced infrared absorption, and surface damage of the silicon wafer is much smaller than that resulting from femtosecond laser irradiation.[35]

C. Reactive ion etching

Reactive ion etching (RIE) is a dry etching technology that uses chemically active gas ions generated by gas discharge to induce chemical reactions on the surface of materials. The principle of reactive ion etching combines physical and chemical etching. The etching gas ($SF_6/CHF_3/O_2$)[36] produces glow discharge under the high-frequency electromagnetic field. F^- ions undergo chemical corrosion with Si atoms to create volatile substances, such as SiF_4. At the same time, O_2 is ionized to generate $O_2{}^-$ ions that combine with Si atoms and F^- ions on the material surface to generate a $Si_xO_yF_z$ passivation layer, which is attached to the tapered sidewall formed by etching. The passivation layer prevents further corrosion and ensures that the etching direction is always vertical to the cross section. The other part of physical etching comes from the sputtering of Si atoms generated by high-energy ion bombardment of the silicon surface. Finally, pyramid-shaped black silicon is formed.

RIE can provide 3D ordered structure arrays with uniform size and depth using a mask. However, to achieve infrared detection and near-zero reflectance across a broad range of wavelengths, the absorption range of black silicon needs to be broadened in RIE by combining with element doping or LSPR.[37]

D. Metal assisted chemical etching

Metal-Assisted Chemical Etching (MACE) is a wet etching technique that utilizes chemical reactions between liquids and solids to etch the surfaces of solid materials. MACE is currently one of the most popular top-down approaches for micro/nanofabrication.[38] The principle of this method is that the metal (Ag, Au, Al, etc.)[39] acts as the cathode, exposed silicon acts as the anode, metal particles play a catalytic role during the etching process, and silicon is exfoliated in the form of SiF_6 ions. Metal particles induce the fast dissolution of the silicon underneath them and move into the bulk silicon in the same direction during etching. The sustained silicon dissolution and concerted movement of metal particles into the bulk silicon eventually lead to the formation of silicon micro/nanostructures, such as nanowires (NWs) and nanoholes.[38]

The surface structure gap of black silicon fabricated by MACE is small, usually tens of nanometers, so it has a high aspect ratio. MACE is advantageous as it is a simple and low-cost method that is suitable for processing nanostructures with large areas.[35] MACE only changes the surface structure of silicon, so black silicon has a good absorption of near-infrared short-wave light (780–1100 nm), which can be enhanced to the absorption of near-infrared long-wave light (1100–2500 nm) by combination with a heterojunction.

III. INFRARED DETECTION APPLICATIONS OF BLACK SILICON

Black silicon has many attractive properties, such as low reflectivity resulting from the micro/nano-structured surface, large chemically active surface area, and ultra-high light absorption in the visible and near-infrared wavelength range imparted by auxiliary materials, e.g., by impurity doping. Therefore, black silicon is a promising material for infrared photodetectors, which overcomes the shortcomings of commercial infrared detectors, such as high cost, high noise characteristics, and poor integration with silicon-based electronic processes, and improves the narrow detection range, low efficiency, and sensitivity of traditional silicon-based photodetectors. In recent years, black silicon based near-infrared photodetectors have been widely explored, mainly by the following strategies: 1. Enhanced photodetectors within the bandgap limit: the photodetectors are aimed at the detection of near-infrared bands below 1100 nm, and black silicon as the substrate is mostly fabricated by MACE and RIE, which can combine with the formation of heterojunctions or other physical processing of materials to enhance the absorption. 2. Enhanced photodetectors above the bandgap limit: the detection range extends above 1100 nm and the used black silicon is mostly fabricated by femto- and nanosecond laser methods. This provides material for developing the silicon-based infrared detection technology, which can be used for silicon-based infrared photodetectors and photodiodes. Both the photodetectors within and above the bandgap limit can obtain higher-performance by deposition of a passivation layer (SiO_2, Al_2O_3, C_3N_4, etc.)[9,40] on black silicon for infrared pixel arrays, room-temperature infrared signal detection, security monitoring, etc. 3. Substrate: black silicon with high optical performance is fabricated, which shows great potential in the application of infrared photodetectors. According to the above content, the performances of all types of black silicon and black silicon photodetectors that include two companies (SIONYX[41] and ELFYS[42]) that have commercialized black silicon photodetectors discussed above are compared in Table I.

A. Basic principle of black silicon based photodetection technology

Photodetectors are based on the basic physical phenomenon of the conversion of light to electricity by photogenerated carriers and usually divided into the two categories: thermal detectors and photon detectors. Photon detectors are based on the photoelectric effect, which is further divided into the external photoelectric effect (photoconductive effect) and the internal photoelectric effect (photovoltaic effect). Photovoltaic detectors with junction structures have been reported to exhibit a faster response speed compared with photoconductive detectors.[70] Black silicon photodetectors are typical photovoltaic photodetectors. When the incident light excites electron–hole pairs, the built-in electric field of the potential barrier separates the electron–hole pairs, resulting in charge accumulation on both sides of the potential barrier, which is called the photovoltaic effect. A potential internal barrier is required to achieve the photovoltaic effect. This potential barrier can be a PN junction, a PIN junction, a Schottky barrier junction, etc. All these junctions are heterojunctions, which are PN junctions formed by two different semiconductor single crystal materials. Compared with homojunctions, these two semiconductors have different bandgaps, resulting in the formation of potential wells on the surface. The confinement effect of the potential wells on the carriers is enhanced, and the heterojunction also has a higher injection efficiency. Heterojunctions[70–74] are the most used junctions in photodetection.

© Author(s) 2023

TABLE I. Performance comparison of black silicon and photodetectors based on black silicon.

Samples	Fabrication method	Spectral range (μm)	Absorptance (%)	Reflectance (%)	Measure condition	Responsivity (mA/W)	Dark current (nA)	References
Black silicon	MACE-Ag	0.4–2.5	A_{max} = 95	⋯	1060 nm	0.57	⋯	43
Black silicon-CZTS	MACE-$HAuCl_4$	⋯	⋯	⋯	800 nm	411×10^{-3}	⋯	44
Black silicon-MoS_2	MACE-$HAuCl_4$	⋯	⋯	⋯	665 nm	1.39	⋯	45
Black silicon	DRIE+PIII	0.4–2.2	62	⋯	1060 nm	0.53	⋯	46
Black silicon	Fs	⋯	⋯	⋯	940 nm	0.55	0.7	47
Black silicon	Fs	⋯	⋯	⋯	1080 nm, V = −5 V	3.23	783	40
Black silicon S-doped	Ns	1.1–2.4	86	⋯	⋯	⋯	⋯	11
Black silicon	Fs	0.25–2	98	⋯	⋯	⋯	⋯	48
Black silicon	Fs filaments	0.2–1.1	90–97	⋯	⋯	⋯	⋯	49
Black silicon Al-doped	Fs	1.5–2.5	60–74	⋯	⋯	⋯	⋯	50
Black silicon Au-doped	Fs	1.1–2.5	60%	⋯	⋯	⋯	⋯	51
Black silicon	Fs	1.1–2.5	>50	⋯	1310 nm, V = −10 V	137×10^{-3}	⋯	52
Black silicon N-doped	Fs	1.1–2.5	20–50	⋯	1310 nm, V = −10 V	5.3×10^{-3}	⋯	53
Black silicon S-doped	Fs	0.4–1.6	⋯	⋯	1080 nm, V = 20 V	1097.60	⋯	54
Black silicon S-doped	Fs	⋯	⋯	⋯	1310 nm, V = −5 V	26.6×10^{-3}	⋯	55
Black silicon Mo-doped	Fs	1.1–2.5	>60	⋯	1310 nm, V = −10 V	76×10^{-3}	⋯	56
Black silicon Te-doped	Fs filaments	0.24–2.5	>85	⋯	808 nm	56×10^{-3}	⋯	57
Black silicon Te-doped	Fs	⋯	⋯	⋯	1120 nm, V = −2 V	120.6	⋯	58
Black silicon Se-doped	Ns	0.4–2.2	81.28	⋯	1060 nm, V = −50 V	0.528	2.8	9
Black silicon-Ag NPs	MACE-Ag	0.8–1.1	80	⋯	1319 nm, V = −3 V	0.277×10^{-3}	⋯	59
Black silicon-PtSi	MACE-Ag	⋯	⋯	⋯	1550 nm, V = −2 V	478.2×10^{-3}	⋯	60
Black silicon	MACE-Al	0.3–1.1	⋯	9.8	⋯	⋯	⋯	61
Black silicon	MACE-Au	0.38–1.05	⋯	0.56	⋯	⋯	⋯	62
Black silicon	MACE-Ag	0.3–1.0	⋯	10	⋯	⋯	⋯	63
Black silicon B-doped	DRIE	5–10	⋯	~0	⋯	⋯	⋯	64
Black silicon	RIE	0.3–2.5	98.9	1.1	⋯	⋯	⋯	65
Black silicon	PIII	0.2–20	>90					3
Black silicon	RIE	0.35–2.5	96.5	⋯	⋯	⋯	⋯	66
Black silicon-Au	RIE	0.22–1.7	⋯	<5	⋯	⋯	⋯	67
Black silicon-NbN	ICP-RIE	1.3–2.5	99.5	⋯	⋯	⋯	⋯	68
Black silicon	ICP-RIE	0.4–1.1	⋯	⋯	⋯	⋯	⋯	69
Black silicon	SIONYX	⋯	⋯	⋯	⋯	⋯	⋯	41
Black silicon	ELFYS	⋯	⋯	⋯	⋯	⋯	⋯	42

Black silicon, as a substrate material, does not directly form a heterojunction, but can form a heterojunction with other materials through element doping or thin film deposition, quantum dots, etc. Element doping brings an intermediate bandgap, and thin film deposition affects the bandgap structure, both of which are equivalent of a decrease of the effective bandgap. In combination with the excellent optoelectronic properties of black silicon, these heterojunctions jointly contribute to the high spectral responsivity, high quantum efficiency, and wide spectral response range of black silicon photodetectors. Taking PN junctions,[75] PIN junctions,[13,43,76] and Schottky barrier junctions[77–80] as examples, the basic principle of the black silicon photodetection technology is briefly described below.

The working principle of the PN junction is shown in Fig. 2(a). When the incident photon energy is higher than or equal to the forbidden bandwidth of the material, it is absorbed by the substrate and excites the valence band electrons in the p and n regions to generate electron–hole pairs. Compared with ordinary silicon-based optoelectronic devices, the unique light-trapping ability of black silicon enhances the initial light absorption, which, in turn, excites more electron–hole pairs. The junction area of the PN junction has a built-in electric field from the n to p regions.[81] Under the action of the built-in electric field, electrons and holes are separated, electrons in the conduction band move to the n region, and valence band holes move to the p region. A higher photovoltage is generated on the two electrodes of the device, and a

© Author(s) 2023

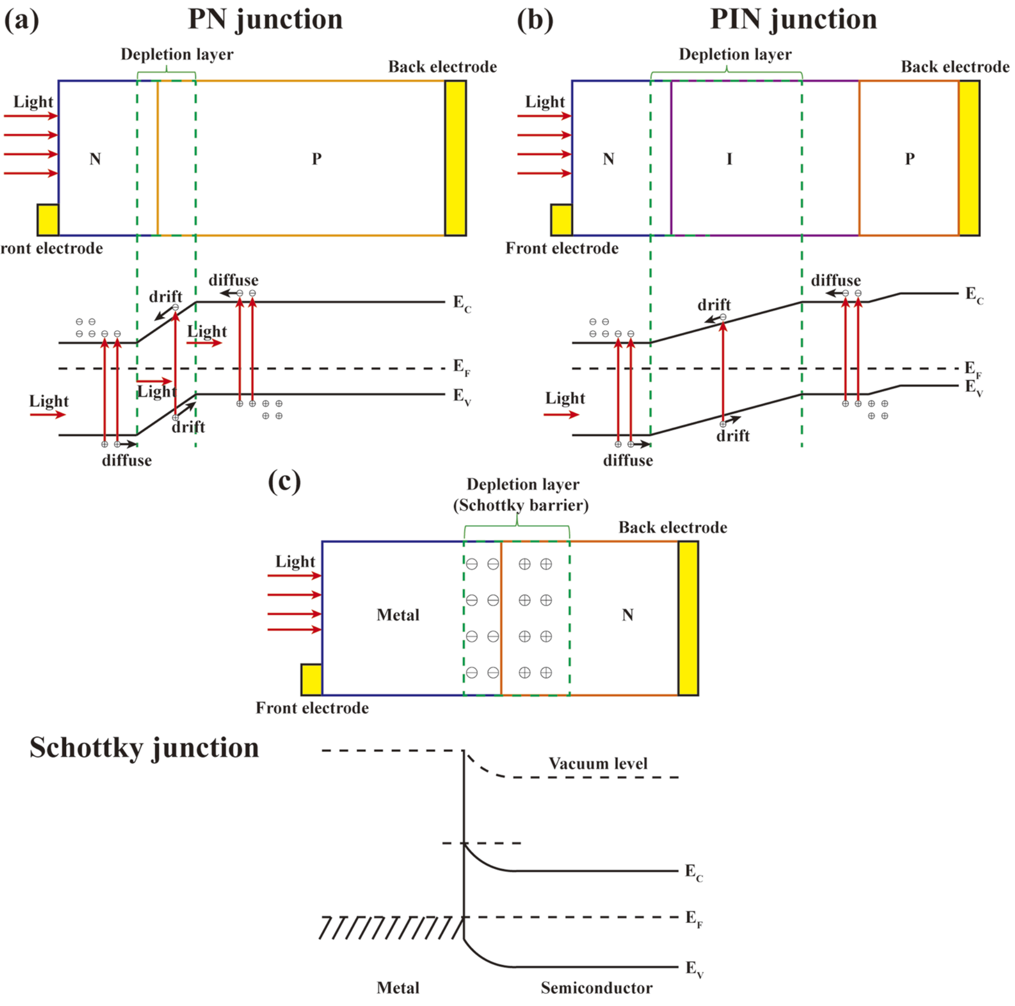

FIG. 2. Schematic diagrams of (a) PN, (b) PIN, and (c) Schottky photodetector structures and their working principles.

stronger photocurrent is formed in the external circuit. Thus, the received optical signal is effectively converted into an electrical output signal, leading to self-powered, fast, broadband, and high responsivity.[72]

The PIN junction is a special case of the PN junction. In contrast to the PN junction, an intrinsic layer I is located between the p and n regions in the PIN junction. The basic principle of the PIN junction is shown in Fig. 2(b). When the PIN junction is illuminated, the light is first transmitted through and reflected from the surface of the device. If the photon energy transmitted through the device is greater than or equal to the forbidden bandwidth, the photon provides energy to the electron in the valence band, enabling electron transition to the conduction band and thus formation of electron–hole pairs. The electron–hole pairs located in the depletion region can be separated by the built-in electric field of the depletion region, pulled to the I and P regions, respectively, and drift toward the electrode. The holes photogenerated in the I region outside the depletion region and the electrons photogenerated in the P region outside the depletion region are minority carriers and reach the depletion region through diffusion. These minority carriers, together with the electron–hole pairs photogenerated in the depletion region, are pulled to the electrodes on both sides under the action of the electric field. All of the carriers are collected to produce a photocurrent. Due to the existence of the I layer, the width of the intrinsic layer of the PIN photodetector is much larger than the space charge region of the ordinary PN junction. As a result, the influence of carrier diffusion movement can be reduced to improve the device sensitivity and response speed.[46]

The PN junction is the contact formed between semiconductors, and the Schottky junction is the contact formed between metal and semiconductor. As shown in Fig. 2(c), determination of the Schottky barrier height is a prerequisite for the engineering of a Schottky junction.[82] Black silicon Schottky barrier photodetectors are usually fabricated using n-type semiconductor Schottky

© Author(s) 2023

junctions. The condition for the formation of the n-type semiconductor Schottky barrier is that the metal work function (W_m) is higher than the semiconductor work function (W_s). When the metal and semiconductor are in contact, a self-built electric field is formed, and the electric field is directed from the semiconductor interior to the surface, forming a surface potential barrier. Upon light irradiation, most photons are directly absorbed by the Schottky barrier. Under the action of the self-built electric field, the electrons cross the Schottky barrier and move toward the semiconductor to generate an electromotive force. The photocurrent is formed by an external electrode to achieve the detection. In contrast to the PN junction, photogenerated electron–hole pairs do not recombine during photoelectric conversion in the Schottky junction, which greatly improves the collection efficiency of the photogenerated carriers, accelerates the response speed, and improves the responsiveness of the device. Therefore, black silicon is used as the substrate to form a heterojunction with other materials, including PN junctions, PIN junctions, and Schottky barrier junctions. Black silicon photodetectors can expand the spectral response range to the near-infrared region for high-performance wide spectral near-infrared detection.

B. Enhanced photodetectors within the bandgap limit

Because of the bandgap limitation of silicon, the enhanced black silicon based infrared photodetectors have high performance in the visible-near-infrared (VIS-NIR) range but only below

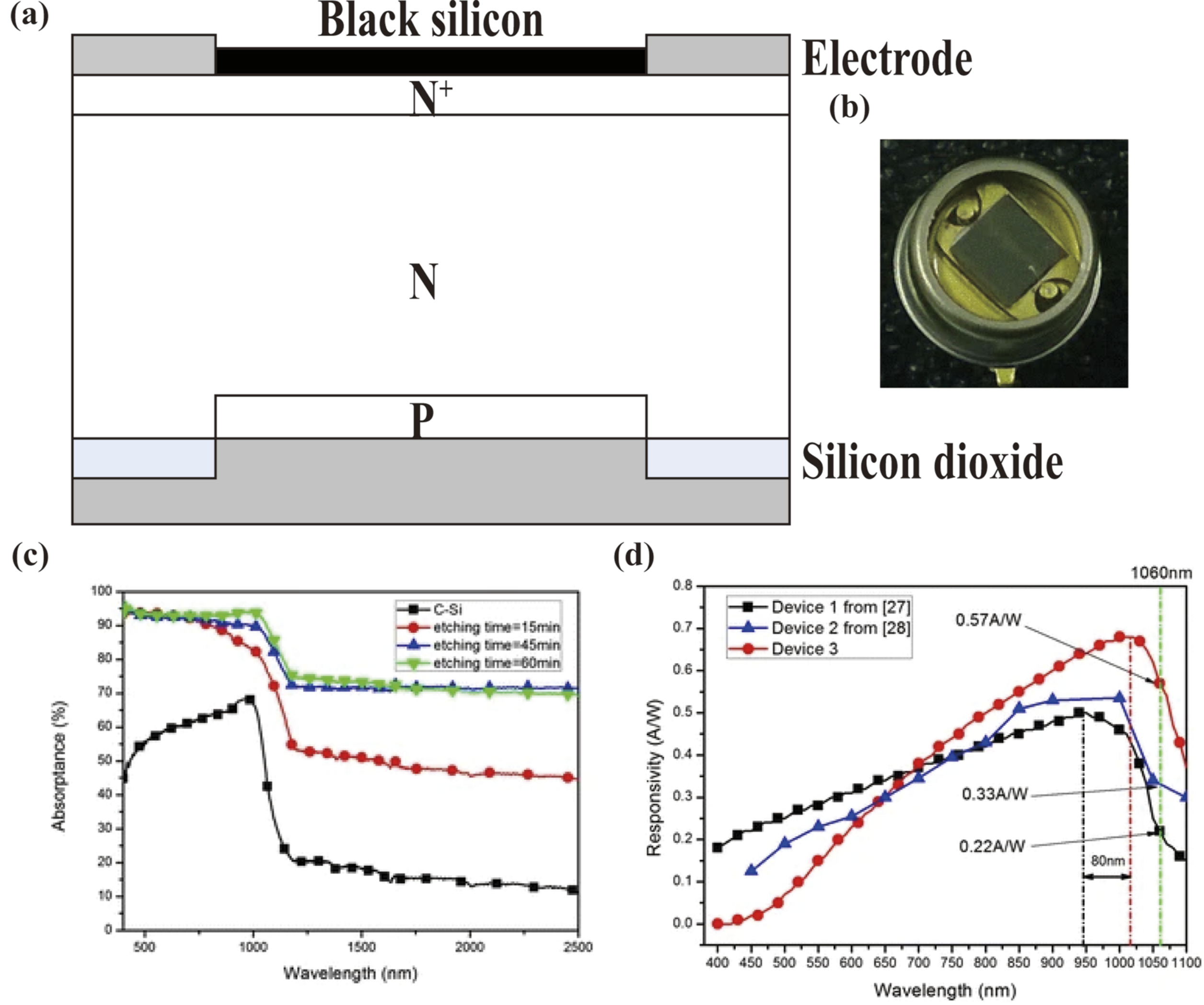

FIG. 3. (a) Structure of the Si-PIN detector based on nanostructured black silicon and (b) photograph of the detector. (c) Absorptance of nanostructured black silicon fabricated at different etching times of 15, 45, and 60 min and C-Si. (d) Responsivities of the Si-PIN detector based on nanostructured black silicon (device 3) and comparison with devices 1 and 2. Reprinted with permission from Wang *et al.*, J. Mater. Sci.: Mater. Electron. **32**(9), 11503 (2021). Copyright 2021 Springer Nature Switzerland AG.

© Author(s) 2023

1100 nm. The photodetectors take advantage of the high absorption within the bandgap of black silicon itself. Black silicon of these photodetectors is mainly fabricated by MACE and RIE and then combining with the formation of heterojunction (MoS_2, $CuZnSnS_4$, etc.) or passivation layer (Al_2O_3, Si_3N_4, etc.) to further improve the near-infrared absorption performance. At the same time, there are also some photodetectors based on black silicon fabricated by femtosecond laser and textured silicon whose device performance is only characterized in the VIS-NIR range. Wang *et al.*[43] used silver ions as catalysts to fabricate novel black silicon-PIN photodetectors on n-type high-resistance silicon substrates (2500–3000 Ω cm) by metal-assisted chemical etching. Figure 3 shows the structure (a) and photograph (b) of the Si-PIN photoelectronic detector with nanostructured black silicon formed on the front surface. The maximum absorption of the device was significantly increased up to 95% in the wavelength range of 400–2500 nm, as shown in Fig. 3(c), and the responsivity was dramatically improved, especially in the near-infrared region, with a responsivity of 0.57 A/W at 1060 nm and 0.37 A/W at 1100 nm, as shown in Fig. 3(d). This black silicon based PIN photodetector has an excellent device performance and potential applications in near-infrared photodetection.

Forming heterojunctions offers a facile route to adjust the spectral response of silicon-compatible photodiodes. Various semiconductor materials with different electrical and optical properties can provide enough flexibility for the design of photoelectric devices.[83] Forming a heterojunction provides a new approach for the development of black silicon based photodetectors for the infrared detection technology. Sarkar *et al.*[45] used $HAuCl_4$ as a catalyst to fabricate nano-cone black silicon on a p-type (100) single-sided polished silicon substrate (resistivity of 1–20 Ω cm) by MACE followed by spin-coating molybdenum disulfide onto colloidal quantum dots (QDs) to form heterojunctions. Figure 4(a) shows the structure of the fabricated photodetector. The fabricated photodetector exhibited a high peak responsivity of 1.39 A/W at 665 nm and 5 V bias, as shown in Fig. 4(b). The combination of MoS_2 quantum dots and black silicon improves the light trapping mechanism, thus producing a broader spectral response and enhanced light absorption. The as-prepared MoS_2QDs/bSi heterojunction broadband (near-infrared-visible) photodetectors have an essential application value for next-generation Si-CMOS-compatible broadband photodetectors using 2D semiconductors. Cu_2ZnSnS_4 (CZTS) nanocrystals have the advantages of low cost and broadband optical

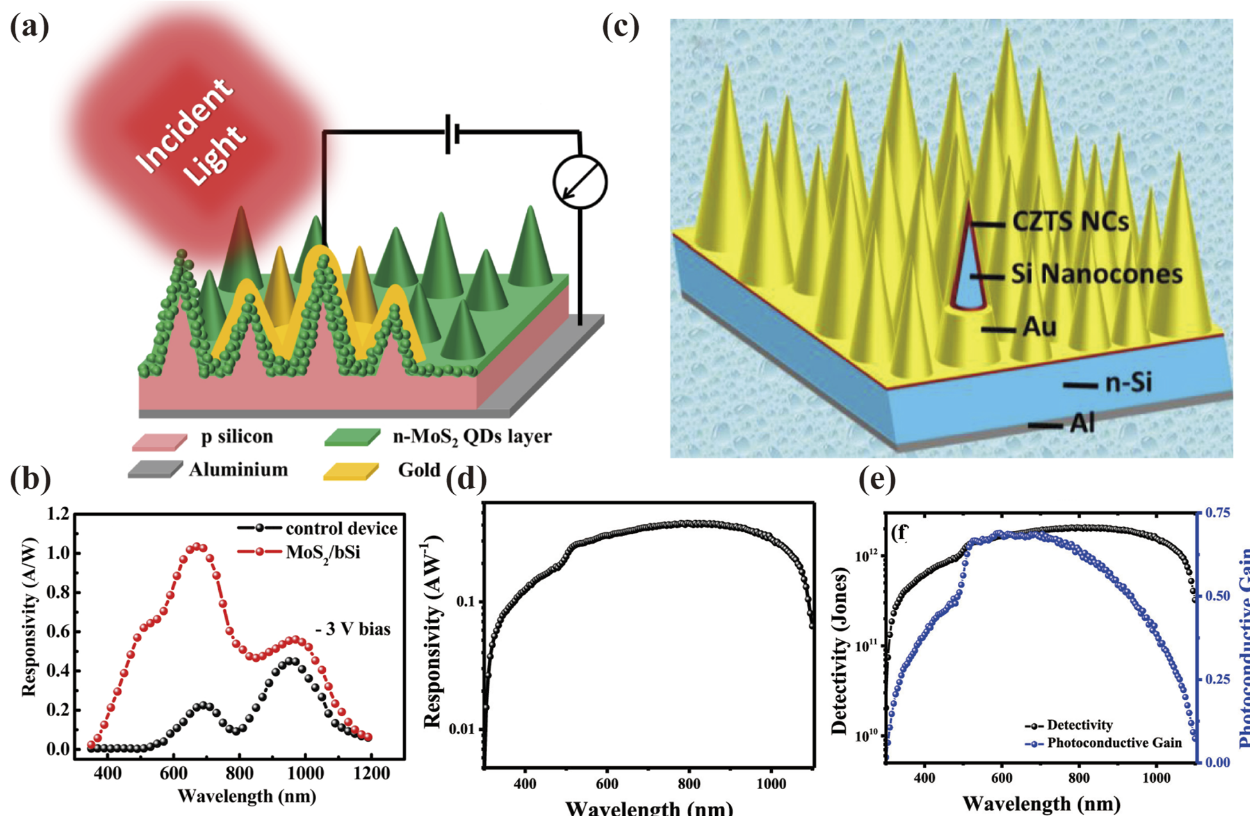

FIG. 4. (a) Schematic of MoS_2QDs/bSi heterojunction broadband photodetectors. (b) Responsivities of MoS_2QDs/bSi hetero-junction broadband photodetectors and the control device. Reprinted with permission from Sarkar *et al.*, Nanotechnology **30**(48), 485202 (2019). Copyright 2019 IOP Publishing. (c) Schematic of b-Si/CZTS heterojunction photodetectors. (d) Responsivity and (e) detectivity and photoconductive gain of b-Si/CZTS heterojunction photodetectors. Reprinted with permission from Singh *et al.*, ACS Appl. Energy Mater. **4**(4), 4090 (2021). Copyright 2021 American Chemical Society.

© Author(s) 2023

absorption properties and can be used as p-type absorption layers in photovoltaic devices. Singh *et al.*[44] first reported a heterojunction formed by black silicon (b-Si) and p-Cu_2ZnSnS_4 nanocrystals (CZTS NCs). $HAuCl_4$ was used as a catalyst to fabricate black silicon on an n-type (100) phosphorus-doped single-side polished silicon substrate (resistivity of 1–10 Ω cm) by MACE. Then, the CZTS NCs were spin-coated to fabricate a b-Si/CZTS heterojunction, producing a self-powered broadband (VIS-NIR) photodetector, and the schematic of the fabricated heterostructure device is shown in Fig. 4(c). The peak responsivity of the photodetector is 411 mA/W [Fig. 4(d)], and the peak detection is 2×10^{12} Jones at 800 nm, as shown in Fig. 4(e). Under optimal conditions, FF (fill factor) of 52%, EQE of 69%, and the power conversion efficiency (PCE) >5% were obtained at a wavelength of 600 nm. The device characteristics show that the heterojunction can be used as a high-performance, self-driven broadband (VIS-NIR) photodetector with high photovoltaic power conversion efficiency.

In addition, defects on the silicon surface will increase the recombination efficiency of photogenerated carriers and reduce the optoelectronic properties of silicon-based devices, so effective surface passivation is indispensable. Common passivation layers include Al_2O_3, TiO_2, and Si_3N_4. Passivation can reduce the spectral reflectance and the recombination rate of photogenerated carriers and significantly improve the device performance, which is beneficial to developing black silicon based photodetectors for an application in the infrared detection technology. As a common method, atomic layer deposition (ALD) was used to deposit dielectric films on black silicon, achieving excellent optical properties and surface passivation for an improved performance of black silicon photodetectors. Heinonen *et al.*[84] established a planar equivalent model of black silicon covered with Al_2O_3 charged films. Black silicon was fabricated by inductively coupled plasma reactive ion etching (ICP-RIE) using 525 μm n-type silicon (>10 kΩ cm) as a substrate. This method enables extensive tuning of the black silicon morphology without causing lattice damage or contamination. The model was then applied to device-level simulations using an inductive junction b-Si photodiode as an example, as shown in the inset of Fig. 5. The model was validated by comparing the simulated QE with experimental results from the same setup. Figure 5 shows that the simulated and experimental QE difference for wavelengths below 1050 nm was less than 1%. In the near-infrared region of 750–1050 nm, the QE was close to 100%. The high density of fixed charges in the dielectric film creates a strong field effect that can play a more active role than pure surface passivation, including the formation of plating or induced junctions in silicon devices. Alumina is a dielectric film with a sufficient amount of negative charges for the creation of a strong built-in electric field for charge separation[83] and can be used as a black silicon photodetector with an induced junction and for the formation of charge carrier PN junctions, which is the most important part for the whole device. Therefore, alumina is a promising material for an application in broadband (ultraviolet to infrared) detection. Zhong *et al.*[46] fabricated black silicon on an n-type high-resistance silicon substrate (2500–3000 Ω cm) by deep reactive ion etching (DRIE) and plasma immersion ion implantation (PIII). By sulfur doping and coating the surface with an Si_3N_4 passivation layer, the obtained Si-PIN photodetector exhibited remarkable device performance, especially in the near-infrared range [800–2000 nm; Fig. 6(a) shows the detector image, and Fig. 6(b) shows the structure of the detector]. Figure 6(c) shows that the maximum absorption reached 83%, and the average absorption reached 62% in the range of 400–2000 nm. The responsivity was 0.53 A/W at 1060 nm and 0.31 A/W at 1100 nm, as shown in Fig. 6(d). This new microstructured black silicon has potential applications in near-infrared photoelectron detection.

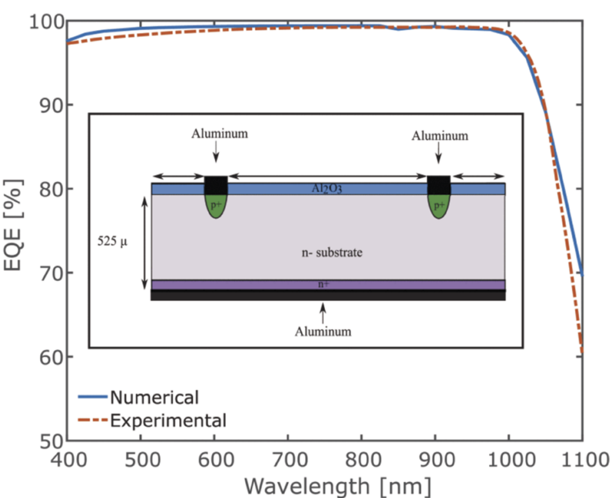

FIG. 5. Comparison of simulated (blue solid line) and experimental (red dashed line) EQE spectra of an induced junction b-Si photodiode verifying the validity of the proposed model. The inset shows a schematic of the structure used to model the operation of the photodiode. Reprinted with permission from Heinonen *et al.*, IEEE Trans. Electron Devices **67**(4), 1645 (2020). Copyright 2020 IEEE.

Near-infrared photodetectors based on black silicon fabricated by femtosecond laser or textured silicon have only characterized their responsivity below 1100 nm and show excellent performance. Zheng *et al.*[47] fabricated a black silicon based photodetector—the all-silicon PIN photodetector GD3252Y—on an N-type high-resistance silicon (2000 Ω cm) substrate using a femtosecond laser, and its structure is shown in Fig. 7(a). The photodetector is deposited with an Si_3N_4 antireflection film on the front side and an SiO_2 passivation film on the backside, which optimizes the surface passivation and reduces the dark current. Figure 7(b) shows that the responsivity in the near-infrared region is increased by about 10% to reach 0.55 A/W, and Fig. 7(c) shows that the quantum efficiency can reach 80%. The peak wavelength is 940 nm, the dark current is only 700 pA, and the response time is 200 ns. The results show that near-infrared absorption, responsivity, and quantum efficiency are significantly improved. The photodetector structure provides a strategy to improve the poor response characteristics of all-silicon detectors in the near-infrared region, which is also of great significance for the development of silicon-based infrared detection. Huang *et al.*[40] used the femtosecond laser to fabricate black silicon (b-Si) on n-type (100) high-resistance silicon (3000–5000 Ω cm) and designed the b-Si photodetector manufactured by a CMOS compatible process as a b-Si-Si lateral heterojunction with a SiO_2 passivation film. Figure 7(d) shows the schematic diagrams of the structure of the b-Si photodetector with a lateral heterojunction. The lateral

© Author(s) 2023

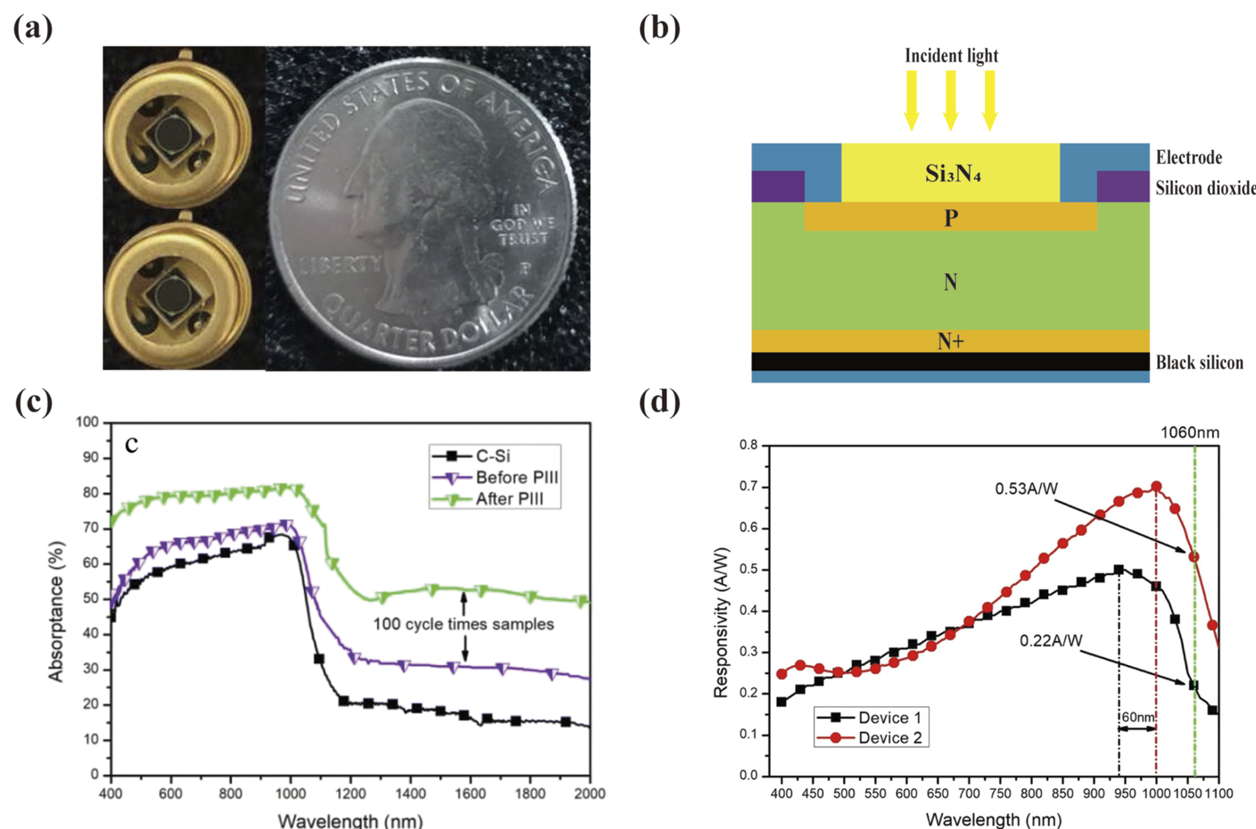

FIG. 6. (a) Photograph, (b) schematic, and (c) absorptance of black silicon fabricated by DRIE before and after PIII and C-Si. (d) Responsivity of the Si-PIN photodetector and comparison with device 1. Reprinted with permission from Zhong *et al.*, Nanoscale Res. Lett. **13**(1), 316 (2018). Copyright 2018 Springer Nature Switzerland AG.

n^+-i heterojunction endows the photodetector with good rectification characteristics. The peak responsivity reaches 3.23 A/W at 1080 nm and −5 V bias, as shown in Fig. 7(e). The b-Si photodetector had a lower dark current (783 nA) compared with the vertical structure and a photocurrent of up to about two or three orders of magnitude. Furthermore, the light–dark current ratio is 155 at the same bias voltage, and the corresponding external quantum efficiency (EQE) reached 371%, as shown in Fig. 7(f). Due to the advantages of low noise, high signal-to-noise ratio (SNR), and high sensitivity, this photodetector has a great potential for infrared pixel arrays and room temperature infrared signal detection.

Zhao *et al.*[85] fabricated a near-infrared (NIR) photodetector based on laser-Si (M-Si) by irradiation of an n-type silicon substrate ($\rho = 4000\ \Omega$ cm) with a nanosecond laser under argon atmosphere, and the structure of this M-Si photodetector is shown in the inset of Fig. 8(a). After annealing, the NIR photodetectors still showed strong sub-bandgap absorption [45.6% at 1310 nm; Fig. 8(a)]. The responsivity was 0.26 A/W at 5 V reverse bias and 8 A/W at 960 nm and 5 V bias, as shown in Fig. 8(b), and the EQE was 1007%. At the same time, the time response of the device was fast with a rise time of 0.13 ms at 900 nm and 3.6 ms at 1310 nm. The photodetector exhibited good rectification properties and a high above/below bandgap photoresponse. Wang *et al.*[86] reported the fabrication of a near-infrared (NIR) photodiode constructed by transferring a single-layer graphene film onto pyramid-structured silicon etched by an aqueous solution. Figure 9 shows the (a) schematic diagram and (b) digital photograph of this photodiode. The assembled device exhibits typical rectification behavior with a rectification ratio of 1.5×10^4. The graphene-pyramid-textured silicon heterojunction shows significant sensitivity to near-infrared light (850 nm) with a responsivity of 20.2 mA/W, as shown in Fig. 9(c). The heterojunction is capable of detecting fast-switching optical signals at frequencies of up to 2000 Hz with rise/fall times of 96/160 s, respectively. The results indicate that this sensitive graphene-pyramid-textured silicon heterojunction photodiode has broad application prospects in future infrared optoelectronic devices.

Recently, the application of optical resonance effects has provided opportunities for silicon-based infrared photodetectors. Optical resonance results from the coupling of light in the cavity through continuous total internal reflection. When resonance occurs in the near-infrared and short-wave infrared (NIR-SWIR) region, photons at the resonance wavelength can maintain at the surface for a long time because they are strongly confined to specific locations where the resonance occurs. This increases the possibility

© Author(s) 2023

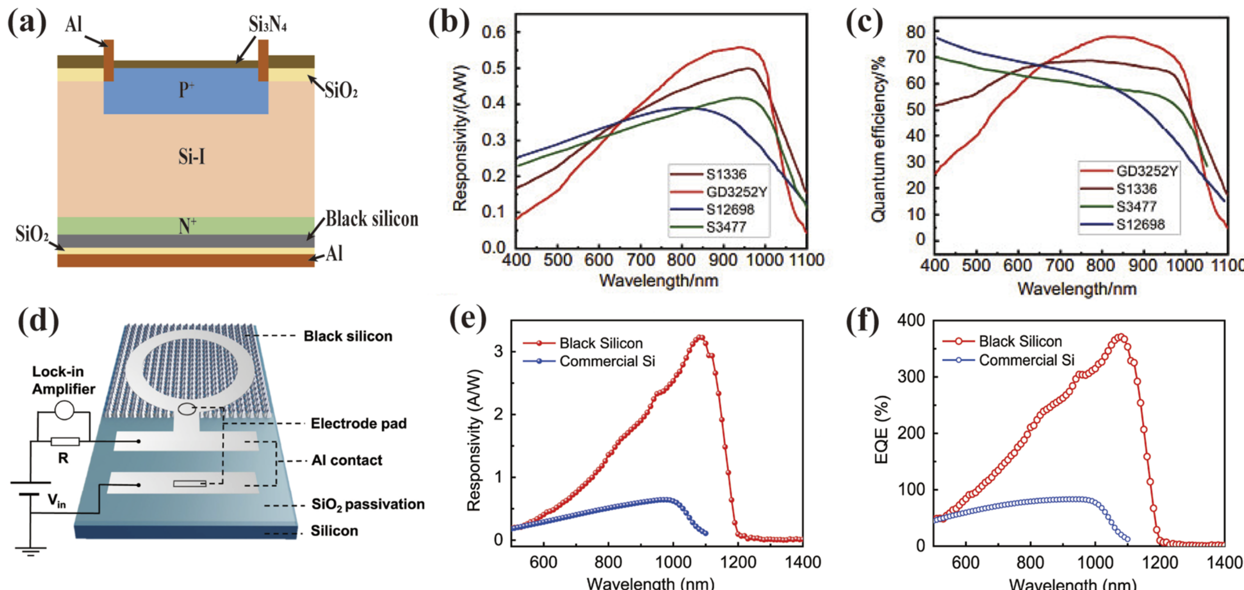

FIG. 7. Schematic diagram, spectral response, and quantum efficiency of different black silicon photodetectors. (a) Schematic diagram of all-silicon PIN photodetector GD3252Y based on the black silicon microstructure. (b) and (c) Responsivity and quantum efficiency of all-silicon PIN photodetector GD3252Y based on the black silicon microstructure and comparison with S1336, S3477, and S12698. Reprinted with permission from Zheng *et al.*, Opto-Electron. Eng. **48**(5), 200364 (2021). Copyright 2021 Opto-Electronic Engineering. (d) Schematic diagram of the black silicon photodetector with a black silicon–silicon lateral heterojunction. (e) and (f) Responsivity and quantum efficiency of the black silicon photodetector with a black silicon–silicon lateral heterojunction and comparison with the commercial silicon photodetector. Reprinted with permission from Huang *et al.*, Opt. Mater. **110**, 110474 (2020). Copyright 2020 Elsevier B.V.

of absorbing NIR-SWIR photons, thereby improving the photocurrent response of silicon photodetectors. Vertical silicon nanowire (SiNW) arrays have the advantage of achieving strong resonant modes over a broad wavelength range from the ultraviolet to a part of the near-infrared region. Kim *et al.*[87] reported hourglass-shaped silicon nanowire-based silicon photodiodes using optical resonance to enhance their photoresponse in the NIR-SWIR region. Hourglass-shaped SiNWs were fabricated on 200 nm silicon wafers (p-type, 8–12 Ω cm) using plasma reactive ion etching (ICP-RIE). Figures 10(a) and 10(b) show that the hourglass-shaped SiNW structure is composed of an upper inverted nanocone structure and a lower nanocone structure, and these two structures synergistically enhance the light absorption in the NIR-SWIR region. The structure of the hourglass-shaped silicon nanowire-based silicon

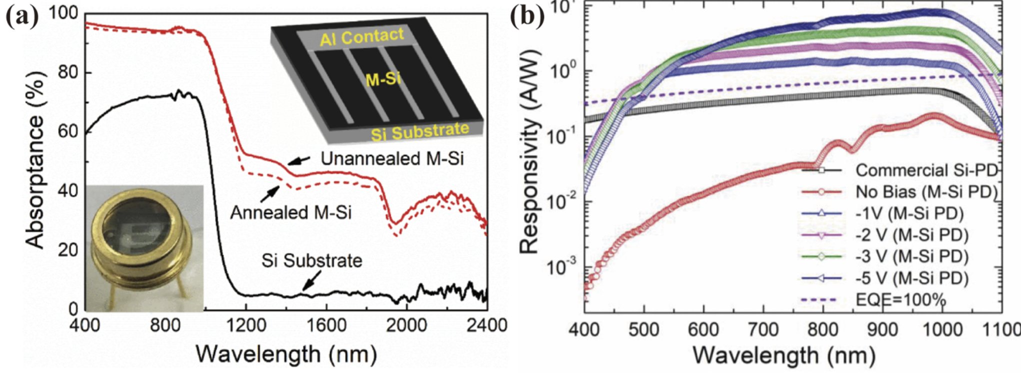

FIG. 8. (a) Absorptance of the M-Si sample before and after annealing in comparison with the absorptance of the Si substrate. Inset: schematic and photograph of the M-Si photodetector. (b) Responsivity of the M-Si photodetector for several reverse biases of no bias, −1, −2, −3, −4, and −5 V, and comparison with the responsivity of the commercial Si photodetector. The relation of EQE of 100% vs the wavelength is shown as a short-dashed line. Reprinted with permission from Zhao *et al.*, IEEE Trans. Electron Devices **65**(11), 4905 (2018). Copyright 2018 IEEE.

© Author(s) 2023

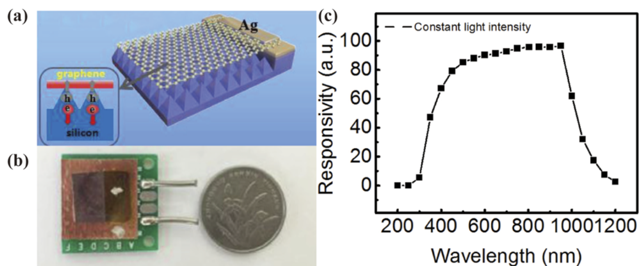

FIG. 9. (a) Schematic diagram and (b) digital photograph of the monolayer graphene-pyramid textured silicon array heterojunction photodiode. (c) Spectral response of a representative graphene-pyramid-textured silicon heterojunction Schottky junction photodiode. Reprinted with permission from Wang *et al.*, Mater. Res. Express **4**(4), 045022 (2017). Copyright 2017 IOP Publishing.

photodiode is shown in Fig. 10(c). Compared with other devices, the hourglass-shaped SiNW device exhibited a responsivity of 0.59 A/W at 1000 nm [Fig. 10(d)]. The highest responsivity of the hour-glass-shaped SiNW device was greater than 70% in the range of 700–1000 nm [Fig. 10(e)], while the EQE of the other devices at all wavelengths was less than 70%. Therefore, the hourglass-shaped SiNW photodetector had the best NIR-SWIR detection performance among all studied devices. This means that the inverted nanocone shape plays a crucial role in the generation of specific optical absorptions caused by whispering gallery mode (WGM) resonances. The use of optical resonance effects to enhance infrared absorption also provides a new approach.

C. Enhanced photodetector above the bandgap limit

It is not enough to achieve high performance within the bandgap. More and more infrared photodetectors still maintain high absorption and responsivity above 1100 nm. Most of the black silicon of these photodetectors is fabricated by femto/nano-second lasers because in different atmospheres (SF_6, N_2, Ar, etc.) or after extra metal film deposition (Au, Al, Mo, etc.), femto- and nano-second lasers can achieve element doping to obtain hyperdoped black silicon. The impurity level of the forbidden band of hyper-doped silicon reduces the bandgap and enhances the absorption of black silicon in the visible and infrared wavelength range to provide

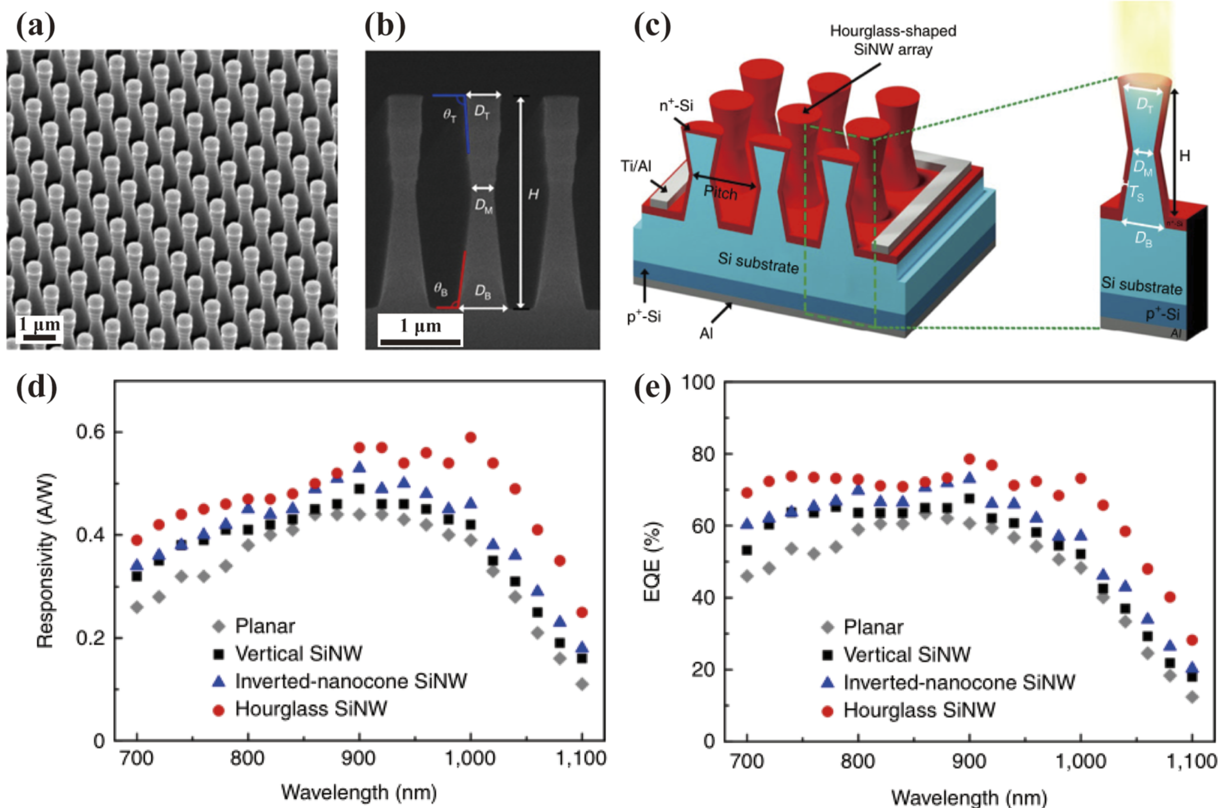

FIG. 10. (a) Tilted view and (b) cross-sectional view SEM images of the fabricated hourglass-shaped SiNW. θ_T and θ_B indicate the outer angles at the top and bottom ends of the nanowire, respectively. (c) Schematic of the hourglass-shaped SiNW photodetector with an enhanced optical response. D_T, D_M, D_B, H, and T_S indicate the top diameter, middle diameter, bottom diameter, height, and thickness of the n^+-Si layer of the hourglass-shaped SiNW, respectively. Comparison of the spectral responsivity (d) and EQE (e) of the hourglass SiNW, planar, vertical SiNW, and inverted-nanocone SiNW photodetector. Reprinted with permission from Kim *et al.*, Nat. Electron. **2**(12), 572 (2019). Copyright 2019 Springer Nature Limited.

© Author(s) 2023

a foundation for the development of the infrared detection technology. However, laser irradiation will damage the black silicon surface, and thermal annealing treatment is often used to reduce and repair the damage of structural defects, aiming to improve the carrier mobility without an evident change of the silicon surface. The annealing temperature and time should also be controlled well because a low annealing temperature does not efficiently reduce the defects, while high-temperature annealing significantly decreases the below-bandgap absorption of micro-textured silicon.[32]

Sulfur-hyperdoped black silicon can be fabricated directly by nano- and femtosecond laser irradiation. Wen *et al.*[11] used silicon ⟨100⟩ wafers (p-type, double-side polished, 4.43 Ω cm) as the starting material. Figure 11(a) shows a side-view SEM image of sulfur-hyperdoped black silicon fabricated using nanosecond laser pulses followed by thermal annealing. The sulfur-hyperdoped black silicon has a higher lattice crystallinity and larger sulfur doping depth than non-doped black silicon. After thermal annealing, the tiny particles and protrusions on the surface of black silicon gradually decreased, and the absorptance reached 86% at 250–2400 nm, as shown in Fig. 11(b). Annealing resulted in good electrical properties as analyzed and tested. After annealing, more S dopants will be activated, which can form covalent bonds with Si to provide more additional free electrons, thus increasing the carrier concentration, reducing the lifetime of minority carriers, and significantly reducing the resistivity and sheet resistance of black silicon. This study shows that nanosecond laser irradiation can be used for the direct fabrication of sulfur-hyperdoped black silicon, which can be used as a silicon-based infrared detection material after thermal annealing. Paulus *et al.*[48] directly fabricated sulfur-hyperdoped black silicon (fs-hSi) on (111) silicon by femtosecond laser irradiation, but laser processing produces harmful amorphous silicon and polysilicon surface layers, which will damage the electronic properties and especially reduce the lifetime of minority charge carriers. Ion beam etching (IBE) can alleviate this problem by increasing the crystallinity of fs-hSi while preserving the tapered microstructure and the infrared absorption properties. Figures 11(c) and 11(d) show the smooth surface obtained by IBE and the flattened tips of the cones. It should be noted that the sulfur doping concentration needs to be kept below 0.6% for a good semiconductor device performance. fs-hSi absorbs photons in the infrared range while exhibiting negligible reflection. The reflectance of fs-hSi is 2%, and the absorptance is 98%, as shown in Figs. 11(e) and 11(f). Combining techniques that produce uniform doping profiles with other annealing techniques, such as nanosecond laser annealing, IBE is a promising laser post-treatment to improve femtosecond laser fabricated black silicon surfaces. It achieves high crystallinity while simultaneously controlling the sulfur concentration in the surface and the thickness of the sulfur-doped layer, thereby enhancing the infrared absorption and providing a reference for the advancement of infrared detection technology.

Using femtosecond laser irradiation, black silicon has been fabricated in near-field experiments reported before, which require the laser beam to be tightly focused on the sample and cannot achieve remote fabrication. Some studies have reported a new

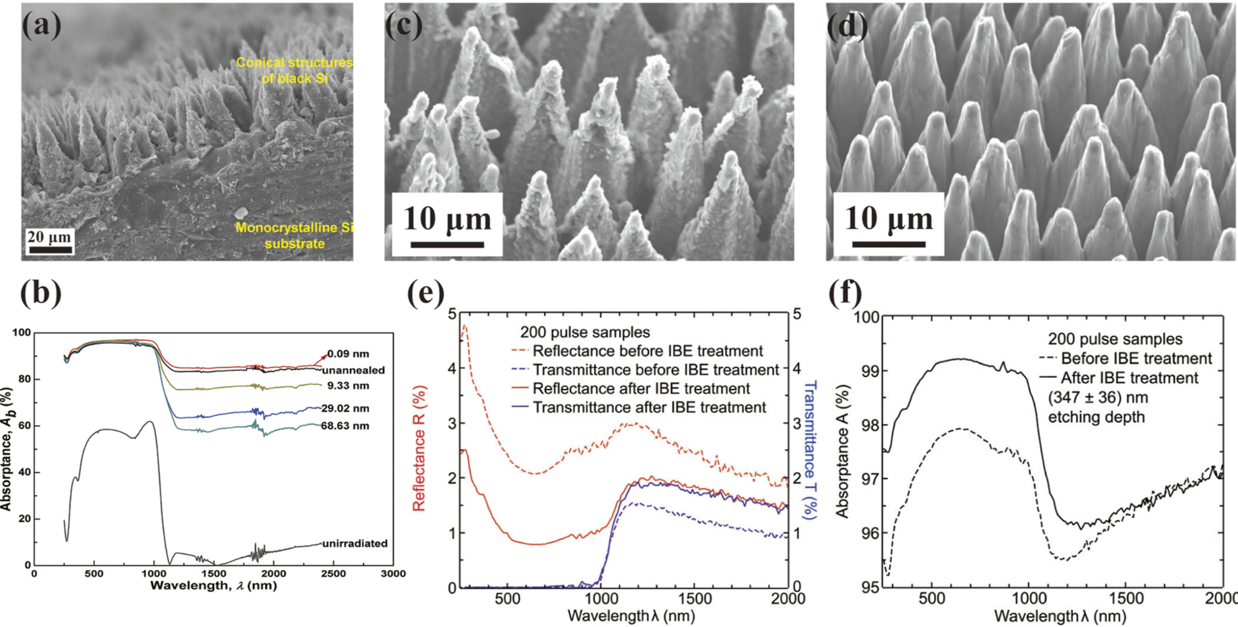

FIG. 11. SEM and optical performances of black silicon fabricated by different laser irradiation methods. (a) Side-view SEM image of black silicon obtained by irradiation with the nanosecond laser. (b) Absorptance of nanosecond laser-fabricated black silicon before and after thermal annealing with S-dopant diffusion lengths of 0, 0.09, 9.33, 29.02, or 68.63 nm. Reprinted with permission from Wen *et al.*, Mater. Res. Bull. **93**, 238 (2017). Copyright 2017 Elsevier Ltd. (c) and (d) SEM, (e) reflectance and transmittance, and (f) absorptance of black silicon using femtosecond laser irradiation in air before and after IBE treatment. Reprinted from Paulus *et al.*, AIP Adv. **11**(7), 075014 (2021) with the permission of AIP Publishing.

© Author(s) 2023

femtosecond laser irradiation technique called femtosecond laser filaments, which can be utilized in the field of remote etching. Zhan *et al.*[49] reported a method for the remote and rapid fabrication of broadband low-reflectivity black silicon by ablating crystalline silicon with femtosecond laser filaments in air, as shown in Fig. 12(a). A porous microstructure is formed on 250-μm n-type (100) silicon as the substrate, which enhanced the light-trapping ability from the ultraviolet to infrared range. The absorbance was 90%–97% for 0.2–1.1 μm, which gradually decreased from 1.1 to 2.5 μm, as shown in Fig. 12(b). Black silicon has similar optical properties to samples fabricated using the traditional femtosecond laser. Femtosecond laser filaments have potential applications in remote and rapid near-infrared detection.

In addition to sulfur doping, femto- and nanosecond lasers can be used to irradiate the silicon surface with a deposited metal film (Au, Al, Mo, etc.) to fabricate hyperdoped black silicon of the corresponding element. Su *et al.*[50] directly irradiated crystalline silicon [n-type (111) double-sided polished silicon] covered by a 100-nm-thick aluminum film with femtosecond laser pulses in air and 1 m, as shown in Fig. 12(c). Al coating was completely removed by secondary ablation and adjusting the process parameters, achieving a 50% increase in absorbance in the SWIR spectral range of 1.5–2.5 μm compared with unsprayed Al coating. The absorption was 90%–96% between 240 nm and 1.0 μm, 65%–74% between 1.2 and 1.8 μm, and 60%–65% between 2.0 and 2.4 μm, as shown in Fig. 12(d). The microstructure formed by laser irradiation leads to an increase in the absorption rate. Al doping leads to a change in the band structure of silicon, so the absorption is enhanced in the short-wave infrared (SWIR) region. It provides an idea for the rapid and economical fabrication of silicon-based optoelectronic devices for the SWIR infrared spectral range. Yu *et al.*[51] first coated a 40-nm Au film on a silicon wafer and then used the femtosecond laser to prepare supersaturated gold-doped black silicon on an N-type (111) high-resistance double-sided polished silicon (1500 Ω cm) substrate. The schematic diagram of the fs laser fabrication system is shown in Fig. 12(e). Black silicon shows high thermal infrared absorption, and Fig. 12(f) shows an absorptance of 60% in the range of 1.1–2.5 μm. At lower laser powers, the Au-induced impurity levels significantly enhanced the IR absorption due to the multiple reflection effect of the geometry. Au doping results in high thermal stability absorptivity. Furthermore, the carrier density is very low due to the self-compensation effect between the donor and acceptor levels of Au. Au also improves the defects of high free carrier absorption and unstable infrared absorption of the sulfur-doped black silicon. Au-doping provides strong support for the infrared detection application of femtosecond laser-irradiated silicon and is a better candidate for the application in infrared detection.

Hyperdoped black silicon is directly prepared using a femto- and nanosecond laser. It is essential to use black silicon as a substrate for the fabrication of optoelectronic devices for infrared detection applications. Li *et al.*[52] fabricated undoped black silicon (b-Si) on an n-type (111) high-resistance silicon substrate (4000 Ω cm) using nanosecond lasers in argon (Ar) atmosphere. The schematic diagram of the photodiodes is shown in Fig. 13(a). Undoped b-Si exhibits over 50% absorption in the range of 1100–2500 nm.

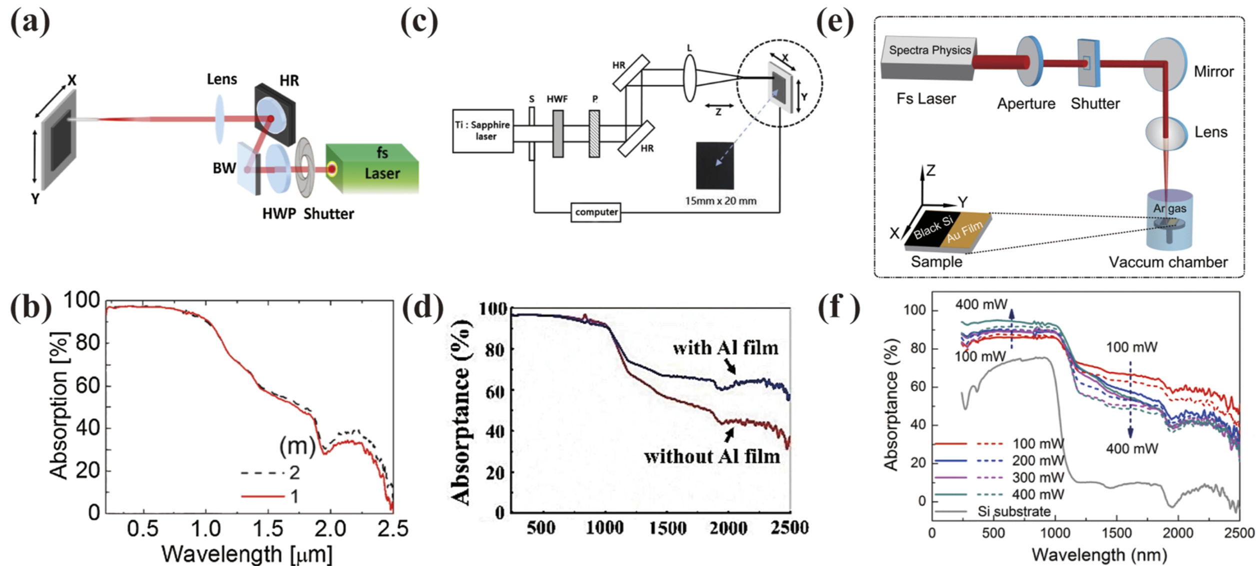

FIG. 12. Schematic diagram of different systems and absorption of black silicon obtained by femtosecond laser irradiation. (a) Schematic diagram and (b) absorption of black silicon using femtosecond laser irradiation in air at 1, 2 m. Reprinted with permission from Zhan *et al.*, Opt. Lett. **42**(3), 510 (2017). Copyright 2017 Optica Publishing Group. (c) Schematic diagram and (d) absorbance of doped black silicon using femtosecond laser irradiation in air with and without the Al film. Reprinted with permission from Su *et al.*, Appl. Phys. B **124**(11), 223 (2018). Copyright 2018 Springer Nature Switzerland AG. (e) Schematic diagram and (f) absorptance of Au-doped black silicon using femtosecond laser irradiation at laser powers of 100, 200, 300, and 400 mW. Reprinted with permission from Yu *et al.*, IEEE Trans. Nanotechnol. **16**(3), 502 (2017). Copyright 2017 IEEE.

© Author(s) 2023

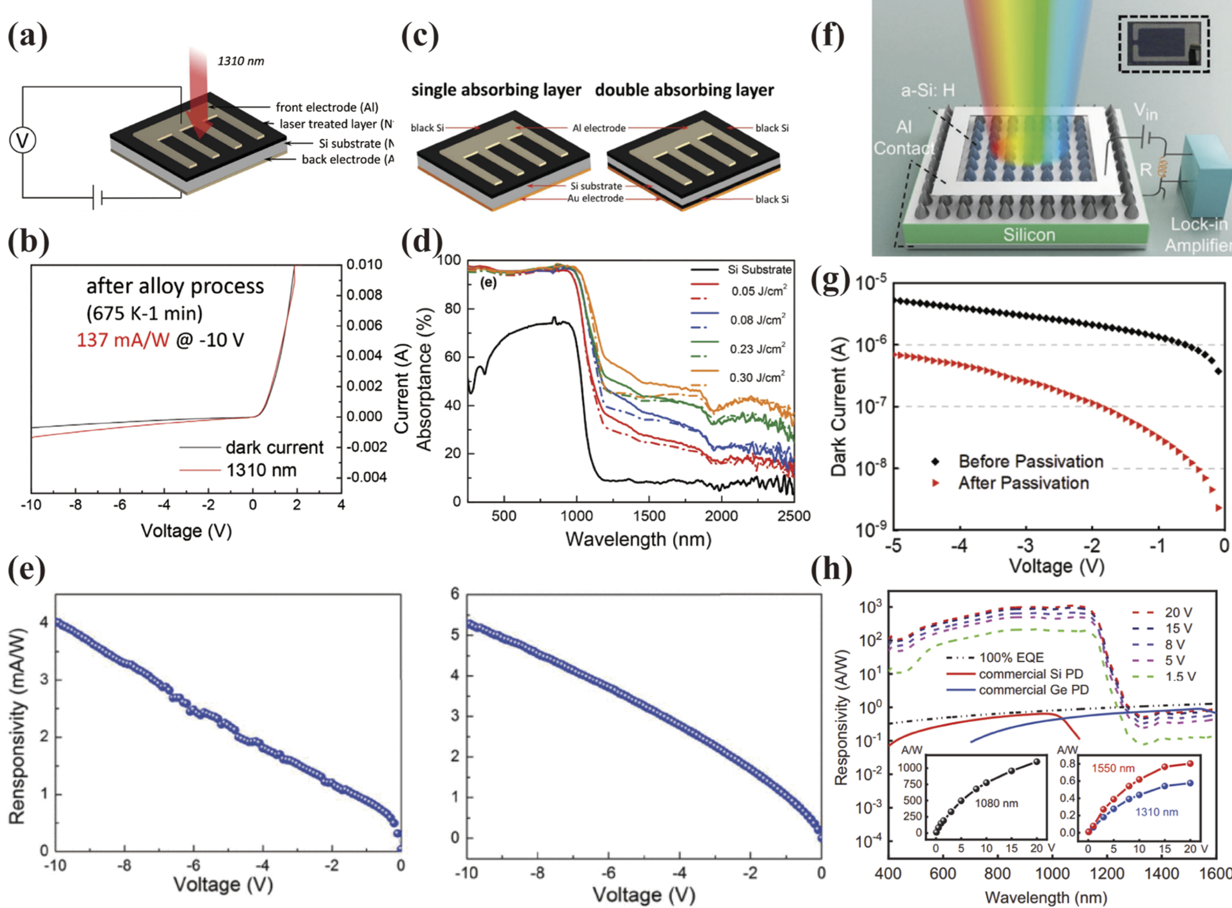

FIG. 13. Schematic diagram, optical performances, and responsivity of different black silicon photodiodes. (a) Schematic diagram. (b) Photoresponse and dark current of non-doped black silicon after the alloy process. Reprinted with permission from Li *et al.*, Opt. Lett. **43**(8), 1710 (2018). Copyright 2018 Optica Publishing Group. (c) Schematic diagram. (d) Corresponding absorptance of nitrogen-doped black silicon at 0.05, 0.08, 0.23, and 0.30 J/cm^2 laser fluence and pristine silicon substrate. The solid lines and dashed lines represent the absorption of unannealed and annealed samples, respectively. (e) Responsivity of single and double absorber layer nitrogen-doped black silicon photodiodes. Reprinted with permission from Li *et al.*, IEEE Sens. J. **18**(9), 3595 (2018). Copyright 2018 IEEE. (f) Schematic diagram of hyperdoped black silicon treated with the surface hydrogenation passivation technology. The inset shows the photograph of the complete detector. (g) Dark current of hyperdoped black silicon before and after surface hydrogenation passivation. Responsivity of different doped black silicon photodiodes. (h) Responsivity of hyperdoped black silicon photodiodes obtained by the surface hydrogenation passivation technology at voltages of 1.5, 5, 8, 15, and 20 V and comparison with commercial silicon and germanium photodetectors. External quantum efficiencies (EQEs) of over 100% were achieved for a wide wavelength range. The insets show the peak responsivity (left) and infrared responsivity (right) against the bias voltage in the range of 0.1–20 V. Reprinted with permission from Huang *et al.*, Adv. Opt. Mater. **8**(7), 1901808 (2020). Copyright 2020 John Wiley & Sons, Inc.

Undoped b-Si has novel optical and electronic properties and is an ideal material for pure silicon-based infrared detectors. Figure 13(b) shows the responsivity of the b-Si photodiode at 1310 nm and 10 V reverse bias, which is as high as 137 mA/W after the alloy process and thus much higher than that of the pure Si photodiode.

The application of hyperdoped black silicon optoelectronic devices in infrared detection is also discussed herein. Li *et al.*[53] fabricated hyperdoped black silicon with excellent infrared properties. They used a femtosecond laser to fabricate nitrogen hyperdoped black silicon on the surface of an n-type (111) single crystal silicon substrate in N_2 atmosphere followed by thermal annealing. Then, they compared the Schottky photodiode with the single black silicon absorption layer and the double black silicon absorption layers. Figure 13(c) shows a schematic diagram of the completed device. Nitrogen-hyperdoped black silicon exhibits significant low-bandgap infrared absorption (20%–50%) at 1.1–2.5 μm, as shown in Fig. 13(d). The single absorber layer photodiode exhibited a low dark current density, good thermal stability, and responsivity of 4.0 mA/W at 1.31 μm and −10 V, as shown on the left of Fig. 13(e). The responsivity could be improved to 5.3 mA/W at the same reverse bias by double absorption layers, as shown on the right of Fig. 13(e). After thermal annealing, the nitrogen-hyperdoped black silicon has strong infrared absorption, a low free carrier concentration, and stable infrared absorption. Therefore, nitrogen-hyperdoped black

© Author(s) 2023

silicon will become a promising material in infrared optoelectronics. Huang *et al.*[54] used a femtosecond laser in combination with the rapid thermal annealing and surface hydrogenation passivation technology to fabricate a hyperdoped black silicon photodetector, and a schematic diagram of the resulting b-Si photodetector is shown in Fig. 13(f). As the substrate, N-type (100) high-resistance silicon (3000–5000 Ω cm) was used. The photodetector has an increased wide bandgap responsivity and signal-to-noise ratio (SNR) and a suppressed dark current. The black silicon photodetector has a spectral range of 400–1600 nm. Figure 13(g) shows that the dark current at −5 V bias is only 7.8 μA. Under a bias voltage of 20 V at room temperature, the responsivity at 1080 nm reached 1097.60 A/W, which is the highest reported responsivity, as shown in Fig. 13(h). The device has an excellent detection capability of 1.22×10^{14} Jones at −5 V. This hyperdoped black silicon photodetector has broad prospects in infrared detection and night vision imaging.

Zhao *et al.*[55] used 250-μm n-type Si(111) (10–15 Ω cm) as the substrate and compared irradiation with the femtosecond laser in the pure SF_6 atmosphere (PD1) and SF_6/O_2 mixed atmosphere (PD2). The schematic diagram of the fs laser fabrication system for S-doped black Si is shown in Fig. 14(a). The device performance of the near-infrared black silicon photodiode was measured [Fig. 14(b)], revealing that PD2 has a responsivity of 11 mA/W at 3 V reverse bias and 1.31 μm, which is 25 times higher than that of PD1 (0.45 mA/W). Furthermore, the responsivity of PD2 increases with the increasing reverse bias voltage of up to 26.6 mA/W at −5 V. This shows that controlling the ratio of O_2 and SF_6 can further improve the near-infrared responsivity of sulfur-doped black silicon. Yang *et al.*[56] used n-type (111) high-resistance silicon (>1500 Ω cm) as the starting material and deposited a 40-nm Mo thin film by magnetron sputtering to fabricate Mo-doped black silicon by femtosecond laser irradiation. The sub-bandgap (1100–2500 nm) absorption of Mo-doped black silicon exceeds 60% at 1310 nm. Finally, a double-junction-based Mo-doped black silicon photodetector was fabricated, as shown in Fig. 14(c). The device can operate under the forward and reverse bias, and the responsivity of the device is 76 mA/W at 1310 nm and −10 V, as shown in the inset of Fig. 14(d). This study demonstrates that the electronic and optical properties of Mo-hyperdoped black silicon make silicon highly competitive for the processing of infrared photodetectors.

In addition to the examples mentioned above, Te can also be used as a doping material for hyperdoping of black silicon. Su *et al.*[57] used Te as a doping element and 470-μm polished N-type (111) silicon wafers (15–30 Ω cm) as the substrate. They first fabricated a photodiode based on black silicon by a femtosecond laser filament, which is a novel femtosecond laser irradiation technique. Filament pulses can deliver constant intensities of 50–100 TW/cm^2 in 100-μm narrow channels to enable the remote and rapid fabrication of a broadband low-reflectivity black silicon surface. The commercial Ti:sapphire laser system and the structure diagram of the silicon photodiode are shown in Fig. 14(e). Figure 14(f) shows that this technology facilitates the fabrication of Te-doped black silicon with

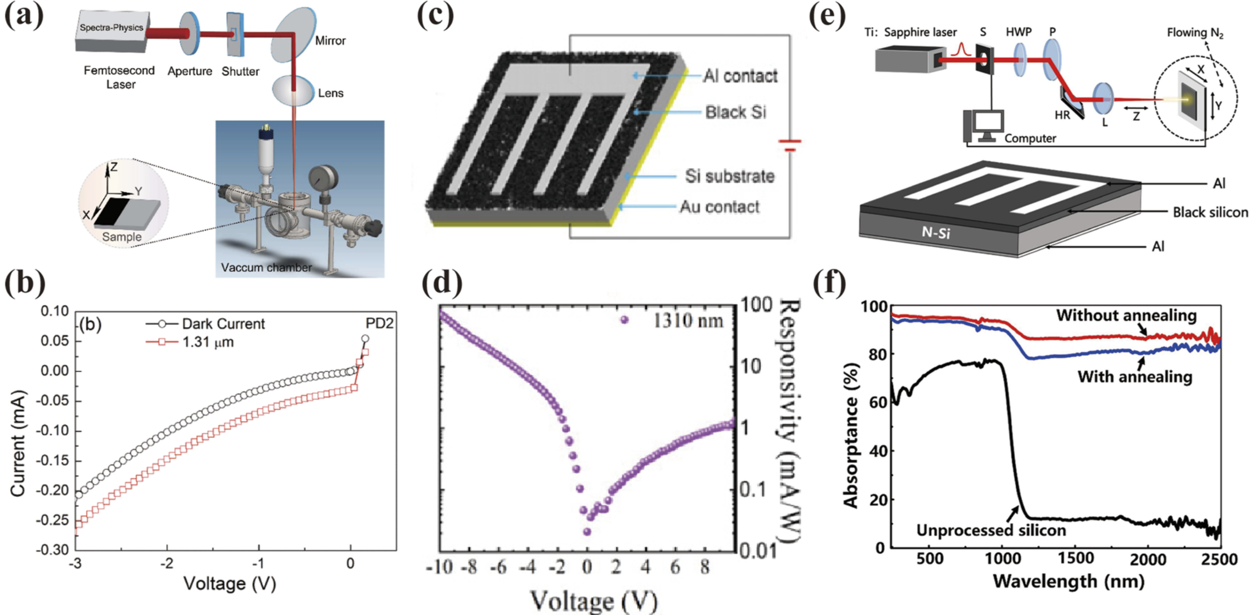

FIG. 14. (a) Schematic diagram of the system of S-doped black silicon fabricated by femtosecond laser irradiation. (b) Photoresponse and dark current of S-doped black silicon PD2. Reprinted with permission from Zhao *et al.*, IEEE Sens. J. **17**, 1000 (2016). Copyright 2016 IEEE. (c) Schematic diagram and (d) responsivity of Mo-doped black silicon photodiodes, respectively. Reprinted with permission from Yang *et al.*, Opt. Lett. **46**(13), 3300 (2021). Copyright 2021 Optica Publishing Group. (e) Schematic diagram of systems and structure of Te-doped black silicon fabricated by femtosecond laser irradiation. (f) Absorptance of Te-doped black silicon with and without annealing and unprocessed silicon. Reprinted with permission from Su *et al.*, Opt. Laser Technol. **123**, 105913 (2020). Copyright 2020 Elsevier Ltd.

© Author(s) 2023

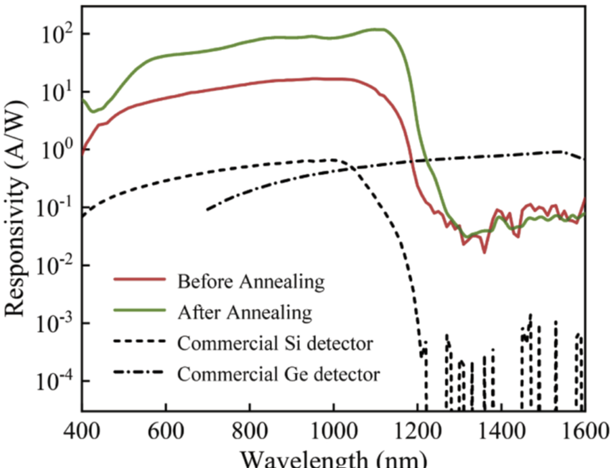

FIG. 15. Responsivity of Te-doped silicon photodiodes before and after annealing and comparison with commercial silicon and germanium photodetectors. Reprinted with permission from Jia *et al.*, Opt. Express **28**(4), 5239 (2020). Copyright 2020 Optica Publishing Group.

an absorption greater than 85% in a wide wavelength range of 240–2500 nm. Therefore, Te-doped black silicon is a good candidate for the fabrication of broadband photodiodes with reasonable rectification and sensitivity properties. The results show that for incident light with wavelengths of 650, 808, and 1550 nm, the responsivity of the Te-doped black silicon photodiode can reach 445, 56, and 15 mA/W, respectively. This demonstrates that the filament processing technique paves the way for the rapid and large-scale fabrication of infrared optoelectronic devices.

The infrared absorption of hyperdoped black silicon prepared by the femtosecond laser method is enhanced. However, the preparation process still introduces a large number of surface defects and forms a large density of surface states on the silicon surface. These surface states can act as recombination centers to promote the rapid recombination of the photogenerated carriers, resulting in a significantly reduced carrier lifetime, which affects the optical and electronic properties. Jia *et al.*[58] fabricated a Te-hyperdoped black silicon photodiode using a 400-μm n-type (100) high resistivity (3–5 kΩ cm) silicon wafer as the substrate with an evaporated 50-nm Te thin film, revealing an unprecedented elevated substrate temperature (700 K) during femtosecond laser irradiation. Figure 15 shows that the photodiode had a responsivity of 120.6 A/W at 1120 nm and 2 V bias after annealing. Noise was highly suppressed, especially in the infrared region. The detectivity (D^*) was about 2.54×10^9 Jones at 1550 nm. Moreover, the responsivity is the highest among Te–Si-based photodiodes and the Te-hyperdoped black silicon photodiode also has a low dark current, low noise, and high stability. The results demonstrate that hyperdoping at high substrate temperature can improve the surface defects due to the femtosecond laser process and has a great potential for the laser-induced modification of semiconductors. Further optimizing the post-processing parameters is expected to result in a better overall performance of infrared photodetectors.

Mi *et al.*[9] used Si_3N_4 as a passivation film in combination with a new process for preparing black silicon for the fabrication of a dual four-quadrant photodetector. Figures 16(a)–16(c) show the schematic structure and physical picture of dual four-quadrant photodetectors. First, a Se film (purity of 99.99%, Se powder as evaporation source) is deposited on N-type high-resistance silicon. Then, the silicon surface was irradiated with a nanosecond laser in an HF atmosphere to fabricate Se-doped black silicon. After annealing at 600 °C, the absorption remained at 81.28% in the range of 400–2200 nm, as shown in Fig. 16(d). The dual four-quadrant photodetector has an average unit response of 0.528 A/W at 1060 nm and 0.102 A/W at 1180 nm and 50 V reverse bias, with an average dark current of 2 nA in the inner quadrant and 8 nA in the outer quadrant. The new process uses a supersaturated Se coating, which reduces the annealing effect on black silicon compared with conventional S-doped silicon. At the same time, surface passivation optimizes the lifetime of minority carriers and reduces the defect density and unnecessary carrier recombination of black silicon. The proposed near-infrared enhanced black silicon dual four-quadrant photodetector is suitable for applications such as infrared night vision detection and applications in the medical fields.

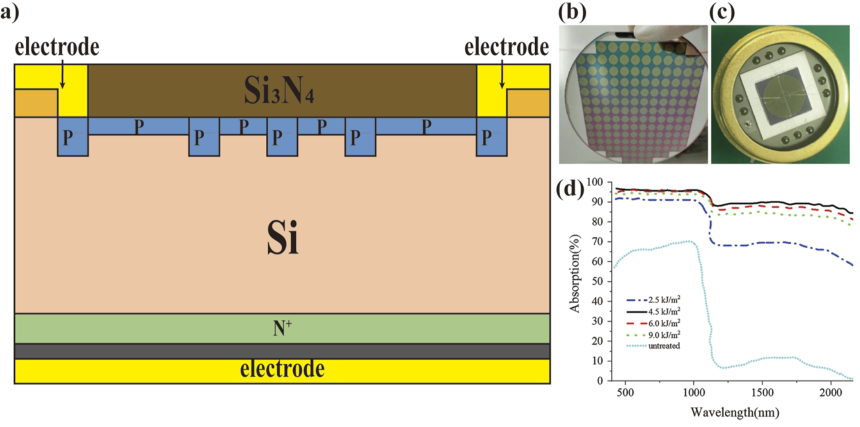

FIG. 16. Schematic diagram, spectral response, and quantum efficiency of different black silicon photodetectors. (a) Schematic diagram. (b) and (c) Photograph of the dual four-quadrant photodetector. (d) Absorption of black silicon of the dual four-quadrant photodetector at 2.5, 4.5, 6.0, and 9.0 kJ/m^2 optical power density and untreated black silicon, respectively. Reprinted with permission from Mi *et al.*, Nanoscale Res. Lett. **16**(1), 38 (2021). Copyright 2021 Springer Nature Switzerland AG.

© Author(s) 2023

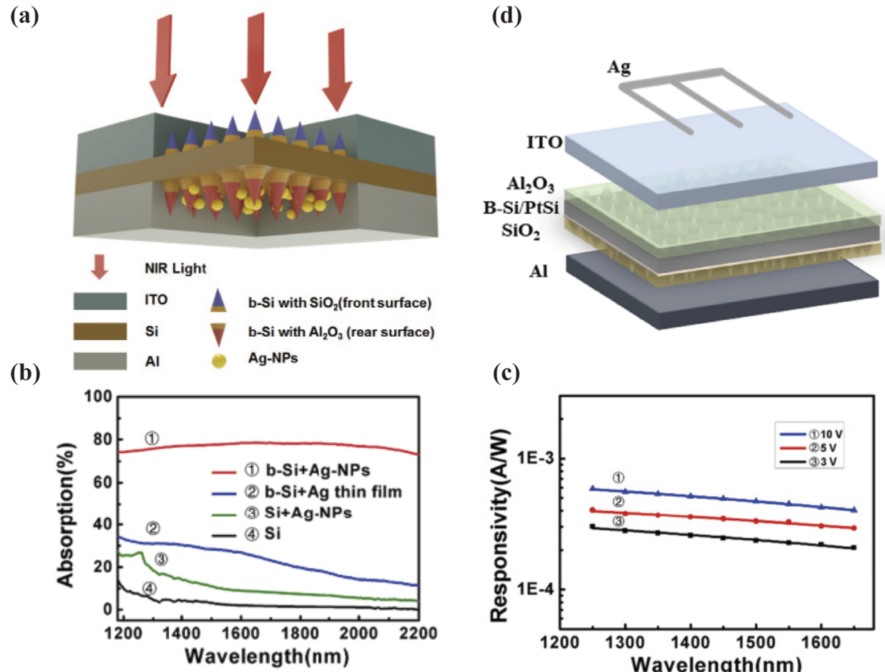

FIG. 17. (a) Schematic of the b-Si/Ag-NPs Schottky photodetector. Absorptance of black silicon + Ag-NPs, the black silicon + Ag thin film, silicon + Ag-NPs, and Si in the wavelength ranges of (b) 1200–2200 nm. (c) Responsivities of the b-Si/Ag-NPs Schottky photodetector at 3, 5, and 10 V, respectively. Reprinted with permission from Hu *et al.*, Opt. Express **27**(3), 3161 (2019). Copyright 2019 Optica Publishing Group. (d) Schematic diagram of the b-Si NIR PD with nano-Schottky detector arrays. Reprinted with permission from Hu *et al.*, Photonics Res. **9**(7), 1324 (2021). Copyright 2021 Optica Publishing Group.

Similarly, black silicon optoelectronic devices fabricated by the MACE also need to be optimized with a passivation layer. Hu *et al.*[59] used Ag nanoparticle catalysts and metal-assisted chemical etching to fabricate black silicon on a (100) high-resistance (5000 Ω cm) double-sided polished silicon substrate. Then, the front surface was coated with an SiO_2 passivation layer and the rear surface was coated with an Al_2O_3 passivation layer. Annealing finally resulted in a silicon photodetector based on a black silicon (bSi)/Ag nanoparticle (Ag-NPs) Schottky junction, and Fig. 17(a) shows the schematic of this b-Si/Ag-NPs photodetector. Ag particles play a role in surface plasmon enhanced absorption. The average absorption of the b-Si/Ag NPs samples reached 80% in the near-infrared region, as shown in Fig. 17(b). The responsivity was 0.277 and 0.226 mA/W at 3 V reverse bias and 1319 and 1550 nm, respectively, as shown in Fig. 17(c), indicating a significantly improved response performance. This simple method provides a new approach for the structural design of silicon-based infrared detectors. Hu *et al.*[60] used metal-assisted chemical etching to fabricate black silicon on both sides of a p-type (100) double-sided polished silicon substrate (resistivity of 5 Ω cm) using Ag as a catalyst and deposited 20 nm Pt on the back of b-Si. An Al_2O_3 passivation layer was formed on the front surface and an SiO_2 passivation layer on the rear surface to fabricate an Si/PtSi nano-Schottky junction silicon photodetector. Figure 17(d) shows the schematic of the b-Si NIR PD architecture with nano-Schottky detector arrays. Table II shows that the highest responsivity was 478.2 mA/W at 1550 nm and −2.0 V, and the specific detection rate was 2.97×10^9 cm $Hz^{1/2}$/W. This work demonstrates a practical room-temperature sub-bandgap near-infrared silicon photodetector with high responsivity and high detection, which can be fabricated conveniently and on a large scale and has a potential practical application value.

Infrared photodetectors based on textured silicon can also achieve high performance above the bandgap. Zhang *et al.*[88] used a 350-μm p-type single-sided polished Si(100) wafer (1–10 Ω cm) as the substrate and studied the broadband infrared responsivity of sulfur-hyperdoped silicon fabricated by femtosecond laser irradiation. The as-prepared PN photodiodes shown in Fig. 18(a) displayed several peaks in the near- and mid-infrared (MIR) regions of the electromagnetic spectrum. At 2.5 V, the dark current density (0.187 mA/cm^2) is reasonable and even better than previously reported dark current densities. Figure 18(b) shows that the sulfur-hyperdoped silicon PN photodiodes exhibit high photocurrents when the photodiodes were illuminated at 1064 nm (below 0.01 W), which may lead to a high photoresponse at near-infrared wavelengths. This technique may provide a promising method for fabricating low-cost broadband silicon-based detectors. Zhang *et al.*[89] fabricated a series of n^+/p photodetectors using hyperdoped silicon fabricated by ion implantation and femtosecond pulsed laser irradiation. In this device, a 300-μm p-type single-sided polished Si(100) wafer (8–12 Ω cm) was used as the substrate, which exhibited a significant enhancement in the absorption and photoresponse at near-infrared wavelengths. The device fabricated with the implantation

TABLE II. Responsivity and specific detectivity of the b-Si NIR photodetector annealed at 950 °C at bias voltages of −1.0, −1.5, and −2.0 V.

Biased voltage (V)	−1.0	−1.5	−2.0
Responsivity (mA/W)	147.6	293.8	478.2
Detectivity (cm $Hz^{1/2}$/W)	9.79×10^8	1.88×10^9	2.97×10^9

© Author(s) 2023

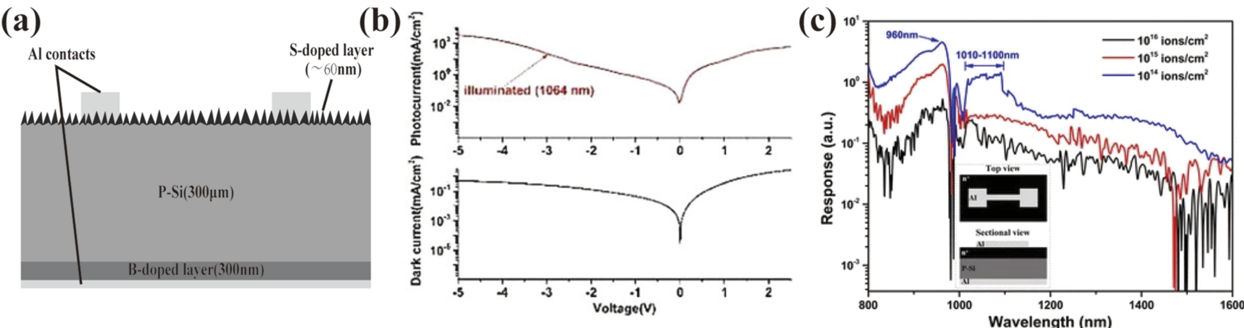

FIG. 18. (a) Schematic diagram and (b) dark current and photocurrent I–V curves of a S-doped silicon photodiode. Reprinted with permission from Zhang *et al.*, Mater. Lett. **196**, 16 (2017). Copyright 2017 Elsevier B.V. (c) Response of n^+/p detectors with different ion-implantation doses of 10^{16}, 10^{15}, and 10^{14} ions/cm^2. The inset shows the top view and cross-sectional view of the device. Reprinted with permission from Zhang *et al.*, Nanoscale Res. Lett. **12**(1), 522 (2017). Copyright 2017 Springer Nature Switzerland AG.

dose of 10^{14} ions/cm^2 showed the best performance, and the responsivity reached a peak at 960 nm, as shown in Fig. 18(d). Pulsed laser melting (PLM) combined with ion implantation is an essential technique for the fabrication of NIR detectors and provides a feasible route to fabricate low-cost broadband silicon-based photodetectors.

D. Promising achievements on black silicon that have potential for photodetectors

To obtain a high-performance infrared photodetector, the performance of the black silicon substrate that is inseparable from the fabrication method is also a key part. Metal-assisted chemical etching (MACE) is a wet etching technique that combines the deposition of metal particles and the etching with a mixed solution of hydrofluoric acid and an oxidant. Common metal particles used as catalysts include Al, Ag, and Au. The MACE method can combine the formation of a heterojunction with other materials to enhance the infrared absorption of black silicon, and the deposition of a passivation layer on black silicon facilitates the fabrication of infrared photodetectors with excellent performance. Uddin *et al.*[61] used the aluminum-assisted chemical etching (AACE) process to fabricate b-Si, wherein 280-μm p-type (100) Cz single crystal silicon (1–10 Ω cm) was used as the substrate, and the thickness of the aluminum (Al) film was 12 nm. Figure 19 shows the top view (a) and cross-sectional view (b) of FESEM images of b-Si fabricated by the AACE process at an annealing temperature of 400 °C. It was found that b-Si nanopores with the deepest nanopores

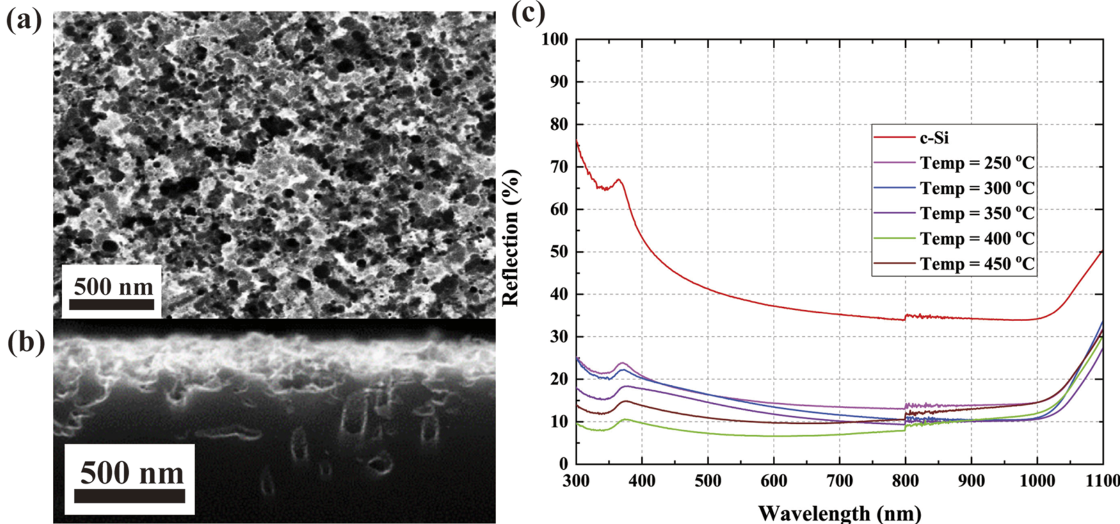

FIG. 19. (a) Top view and (b) cross-sectional view of FESEM images of b-Si fabricated by the AACE process at an annealing temperature of 400 °C. (c) Reflection profiles of b-Si fabricated at different annealing temperatures (250–450 °C) in the wavelength range of 300–1100 nm and comparison with c-Si. Reprinted with permission from Uddin *et al.*, Mater. Sci. Semicond. Process. **133**, 105932 (2021). Copyright 2021 Elsevier Ltd.

© Author(s) 2023

(average depth of 256 nm) and the highest surface coverage (49%) were formed after annealing at the optimal temperature of 400 °C. The broadband reflectance of black silicon was reduced to 9.8% in the range of 300–1100 nm, and R_{min} was reduced to 6.6%, as shown in Fig. 19(c). The highest average absorption enhancement of 1.61 was achieved, which shows that the AACE process provides a low-cost fabrication method to achieve silicon with high absorption in the near-infrared region.

Franz *et al.*[62] fabricated high-aspect-ratio black silicon by the MACE method using a 150-μm phosphorous-doped (5–20 Ω cm) silicon (100) wafer as a substrate. The morphology and reflectivity of black silicon in the presence of different noble metal nanoparticle catalysts (Au, Pt, Pd, Cu, and Ir) were investigated. Wafers were coated with 5-nm thin films of noble metals using standard Physical Vapor Deposition (PVD) methods, followed by thermal annealing under vacuum to form particles. The selection of noble metals and the formation process of noble metal particles play an important role in the overall integration. Figures 20(a)–20(e) show the SEM image of the etched structures prepared with Au particles. Using Au results in vertical structures, whereas etching using platinum group metals (Pt, Pd, or Ir) produces mainly nanoporous sponge-like structures. Figure 20(f) shows the reflectivity of black silicon prepared with Au nanoparticles for visible and near-infrared light (380–1050 nm). Wafers etched in the absence of H_2O_2 showed a high reflectivity of about 34%. When a 50 mmol/l H_2O_2 solution was used, a flat and uniform absorption behavior with an average reflectance of only 0.56% was observed. The Au catalyst shows a lower reflectivity to near-infrared light than other noble metal nanoparticles, which provides a basis for the realization of black silicon based infrared detection.

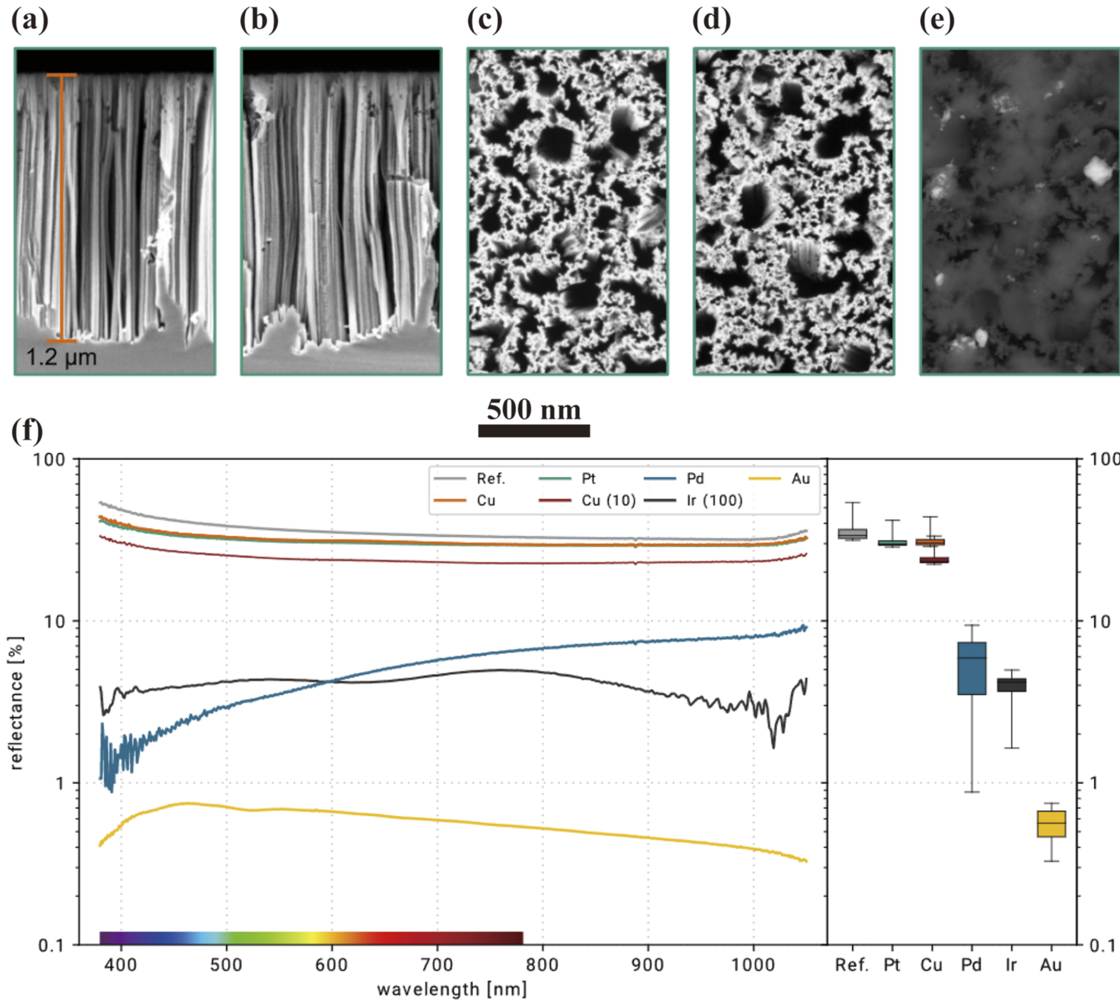

FIG. 20. SEM images of etched structures (with 50 mmol/l H_2O_2 and 1.73 mol/l HF for 10 min) using Au particles. (a) and (b) Cross section, (c) and (d) top view, and (e) top view from the back-scattering detector with highlighted Au particles. The scale applies to all images. (f) Reflectance of fabricated 3D templates etched with 50 mmol/l H_2O_2 and 1.73 mol/l HF for 10 min. The spectra of a Si reference, of a Cu wafer etched with 10 mmol/l H_2O_2, and of an Ir sample etched with 100 mmol/l H_2O_2 are given for comparison. Reprinted with permission from Franz *et al.*, Beilstein J. Nanotechnol. **11**, 1439 (2020). Copyright 2020 Beilstein-Institut.

© Author(s) 2023

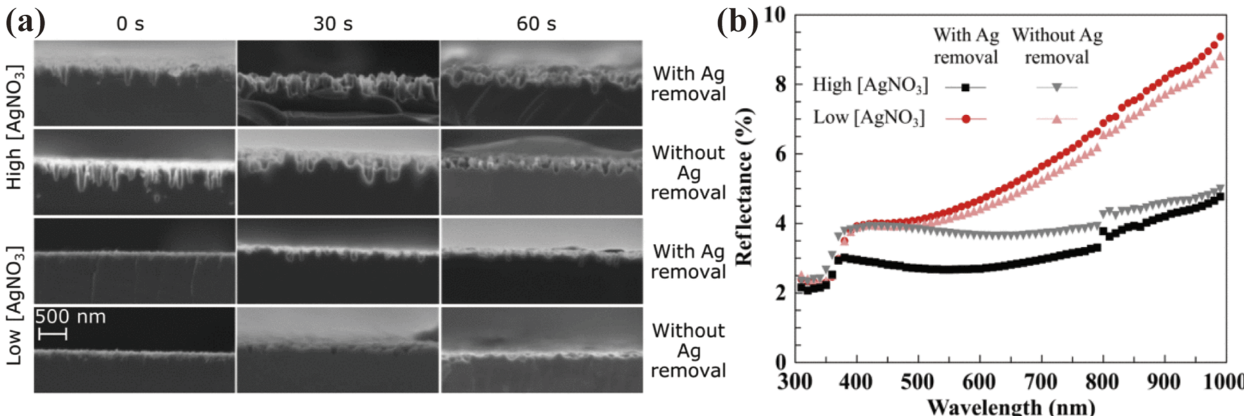

FIG. 21. (a) SEM images of the ALD Al_2O_3-coated b-Si samples prior to and after 30 or 60 s polishing. A higher $AgNO_3$ concentration in the first step resulted in needle-shaped nanostructures, whereas a lower $AgNO_3$ concentration produced a nanoporous surface. Polishing reduced the size of the nanostructures in all samples. The same scale bar applies to all images. (b) Reflectance spectra of b-Si samples prior to polishing. The nanostructure of the samples is coated with ALD Al_2O_3. The spikes at the wavelength of 800 nm result from the change of a grating. Reprinted with permission from Chen *et al.*, IEEE J. Photovoltaics **9**(4), 974 (2019). Copyright 2019 IEEE.

MACE facilitated the fabrication of black silicon with low reflectivity in the near-infrared region, but chemical vapor deposition (CVD) of silicon nitride (Si_3N_4) is performed to achieve better surface passivation at the expense of excellent optical properties. Chen *et al.*[63] proposed to perform atomic layer deposition (ALD) of Al_2O_3 instead of CVD Si_3N_4 by using quarters of a 4-in. shiny-etched boron-doped p-type high-quality float-zone silicon wafer [1 Ω cm, 250 μm, (100) orientation] as the starting material to fabricate black silicon by MACE. The effects of the silver nitrate concentration, silver removal, and polishing on the optical and electrical properties of b-Si were investigated. Figure 21(a) shows the cross-sectional SEM images of the b-Si samples prior to (0 s) and after 30 or 60 s of polishing. Figure 21(b) shows the reflectance spectrum of the unpolished b-Si sample. All samples showed less than 10% reflectance over the entire detection wavelength range between 300 and 1000 nm. In particular, the maximum reflectivity of the high-concentration silver nitrate sample was only 4%. The results demonstrate that ALD Al_2O_3 omits the traditional polishing step and is also compatible with various surface morphologies due to its excellent shape retention, thus allowing for more flexibility in tuning the MACE parameters. At the same time, a low reflectivity in the near-infrared region is achieved.

Reactive ion etching (RIE) is also a commonly used method for the fabrication of black silicon, combining element doping, LSPR effect, and a passivation layer for the fabrication of black silicon based infrared photodetectors. Ryu *et al.*[64] fabricated nanostructured V-groove black silicon (b-Si) by deep reactive ion etching (DRIE). Figure 22(a) shows that the nanoscale V-groove height

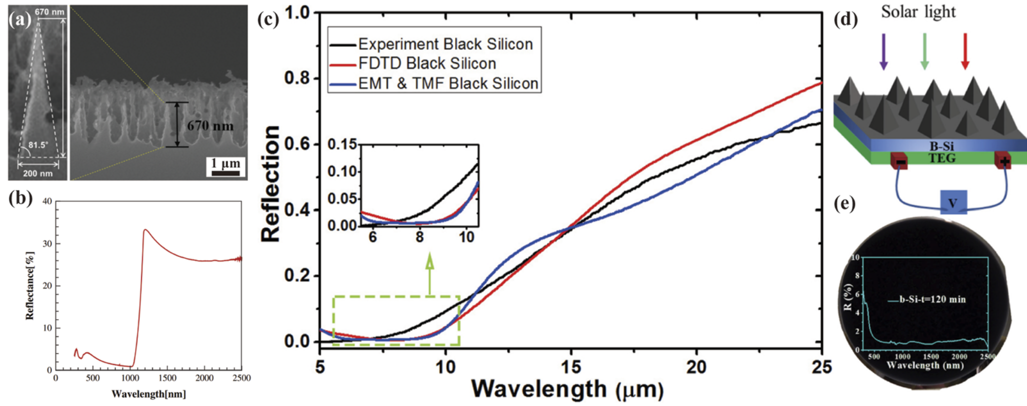

FIG. 22. (a) Cross-sectional view and (b) reflectance spectra of nanostructured V-groove black silicon. Reprinted with permission from Ryu *et al.*, J. Nanosci. Nanotechnol. **19**(4), 2202 (2019). Copyright 2019 Ingenta. (c) Experimental, simulated, and analytical reflection spectra of the fabricated black silicon. Reprinted with permission from Gorgulu *et al.*, J. Opt. **19**(6), 065101 (2017). Copyright 2017 IOP Publishing. (d) Schematic of black silicon nanopyramids. (e) Reflectance spectra of black silicon nanopyramids with 120 min etching time. Reprinted with permission from Cheng *et al.*, ACS Appl. Mater. Interfaces **13**(1), 1818 (2021). Copyright 2021 American Chemical Society.

© Author(s) 2023

and diameter are about 670 and 200 nm and that the grooves are evenly distributed on the surface of the b-Si wafer. In the wavelength range of 250–2500 nm, the reflectance of b-Si as a function of the wavelength is shown in Fig. 22(b), and the reflection of black silicon is close to zero in the wavelength range less than 1 μm. This result implies that b-Si nanostructures have been successfully applied in the near-infrared range. The reflectivity increases sharply at wavelengths above 1 μm; thus, the fabricated b-Si is unusable at wavelengths above the mid-infrared region. Gorgulu *et al.*[90] studied the absorption of mid-infrared light by low-resistivity black silicon fabricated by deep reactive ion etching (DRIE). A 500 ± 20 μm Czochralski-grown ⟨100⟩ silicon wafer (0.001–0.002 Ω cm) with a boron-doping concentration of 7.5 × 10^{19} cm^{-3} was used as the substrate. The fabricated black silicon had a pyramid structure with the height of several micrometers and the width of several hundred nanometers (100–300 nm), which was simulated using the finite difference time domain (FDTD) method. Figure 22(c) shows the reflectance of the experimental black silicon, FDTD simulation, and effective medium theory (EMT) and transfer matrix formalism (TMF) black silicon. The simulation and analytical results are all good estimates of the experimental results. The investigated structures revealed that the fabricated black silicon is a broadband all-silicon infrared absorber for infrared imaging. Cheng *et al.*[65] fabricated highly conductive black silicon (b-Si) with no apparent optical bandgap by reactive ion etching (RIE) using (525 ± 20) μm p-type (100) doped Si (0.01–0.02 Ω cm) as the substrate. The b-Si nanopyramids have a height of 407 nm and a tilt angle of about 60°, and the schematic of the black silicon nanopyramids is shown in Fig. 22(d). They can absorb a large amount of light in a wide range of wavelengths, and the absorption reaches 98.9% even in the near-infrared region (~2500 nm). The optimized b-Si shows less than 0.1% specular reflection [Fig. 22(e)] and mostly less than 2% (average reflectance around 1.1%) total reflection (incident reflection + diffuse reflection) between 300 and 2500 nm, corresponding to an excellent light-trapping ability. The high NIR absorption beyond the band edge is caused by the combination of high doping density and nanostructure. High doping concentration introduces impurities. Due to the presence of impurities, an intermediate bandgap is introduced in silicon, which is equivalent to decrease the effective bandgap of silicon. Thus, the electrons can be excited by light with lower energy and transition easier, realizing the infrared absorption above the bandgap.

Sarkar *et al.*[3] used a 525 μm (100) single polished silicon wafer, with n-type phosphorous doping at a measured resistivity of 0.0015 Ω cm as substrates. Using the ICP-RIE technology to obtain an ultrabroadband, ultrablack silicon surface, the absorption is as high as 99.5% in 1–8 μm, and it is still more than 90% until 20 μm, as shown in Fig. 23(a). Different from the traditional etching technology, the experiment was performed at very low temperatures of −110 °C. The etching resulted in tapered nanostructures with very high aspect ratios, up to 30:1, and a depth of 10.3 μm, as shown in Figs. 23(b) and 23(c). The specific high-aspect-ratio conical geometry of the black silicon surface, combined with the high doping (5 × 10^{19} cm^{-3}) of the silicon bulk, is a key parameter for obtaining the excellent infrared absorption of black silicon. Reportedly, exceptionally high absorbance in the mid-infrared (MIR) also translates into high emissivity for doped black silicon. This article reveals that both highly doped and deep black silicon are favorable candidates for applications such as radiative cooling, broadband absorbers for infrared radiation sensors, and broadband infrared light sources.

Besides element doping, the combination of black silicon and LSPR can also result in an increased infrared absorption. Localized Surface Plasmon Resonance (LSPR) occurs when the frequency of incident light on nanoparticles matches with vibrational frequencies. As a result, nanoparticles or metal islands strongly absorb photon energy. Various noble metals (Au, Ag, etc.) form nanoparticles, but most studies of the LSPR effect are performed on Au particles. Song *et al.*[66] modified densely disordered gold nanoparticles (AuNPs) on a black silicon (b-Si) nanostructure (without self-assembly by photolithography), which was fabricated by reactive ion etching (RIE). As the substrate, a p-type (100) double-sided polished silicon wafer was used (10–15 Ω cm). Figures 24(a)–24(c) show that b-Si has a unique geometry consisting of sharp "needles" at the top and round "holes" at the bottom and are perfectly adapted to gold deposition. The results show that absorption of 96.5% is achieved under optimal conditions in the range of 350–2500 nm, as shown in Fig. 24(d). Black silicon can be applied to near-infrared sensitive

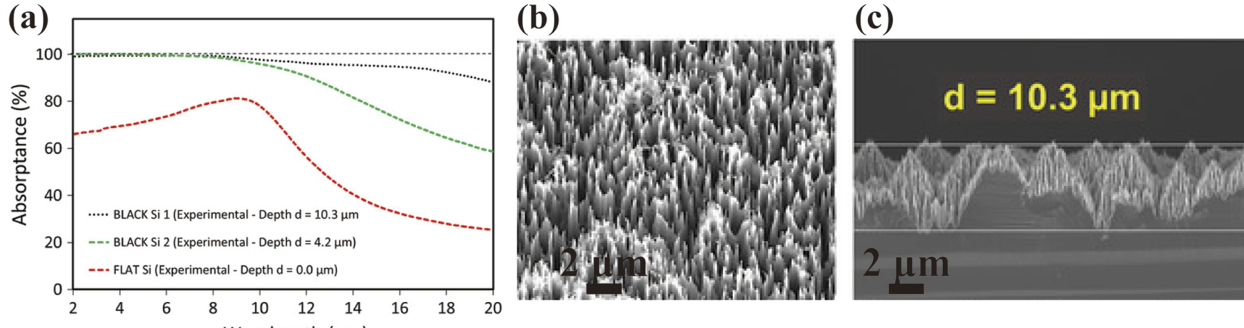

FIG. 23. (a) Experimentally measured spectral absorptance on three samples of UB-B-Si exhibiting different average depths of ⟨d⟩ = 10.3, 4.2, and 0.0 μm (flat surface), respectively, recorded at 15° incidence angle. (b) Top view and (c) cross-section SEM images of ultrablack silicon fabricated by the ICP-RIE technology. Reprinted with permission from Sarkar *et al.*, Adv. Photonics Res. **3**, 2200223 (2022). Copyright 2022 John Wiley & Sons, Inc.

© Author(s) 2023

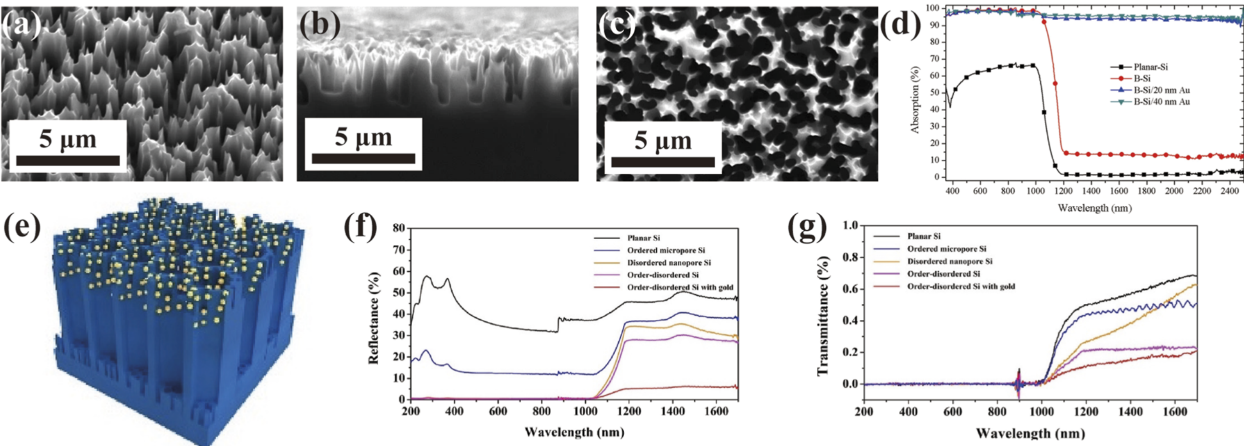

FIG. 24. (a) Top view at a 30° angle and (b) cross-sectional and (c) top view SEM images of the black silicon nanostructure fabricated from RIE at 60/55 SCCM SF_6/O_2 mixtures. (d) Absorption of the black silicon nanostructure with 20 and 40 nm Au, planar-Si, and b-Si. Reprinted with permission from Song *et al.*, J. Mater. Sci.: Mater. Electron. **31**(6), 4696 (2020). Copyright 2020 Springer Nature Switzerland AG. (e) Schematic of order–disordered Si modified with gold. (f) Reflectance and (g) transmittance spectra of order–disordered Si with gold, planar Si, ordered microporous Si, disordered nanoporous Si, and order–disordered Si. Reprinted with permission from Zhang *et al.*, Nano Energy **65**, 103992 (2019). Copyright 2019 Elsevier Ltd.

optoelectronic devices for high-performance detection. At the same time, the significantly enhanced near-infrared absorption of LSPR is also of great importance for infrared photodetection. Zhang *et al.*[67] proposed a new structure of black silicon, which combines ordered micropores and disordered nanopores. Black silicon was fabricated on ap-type ⟨100⟩ silicon substrate (10–30 Ω cm) by a two-step etching method. The first step involved mask-assisted reactive ion etching to form ordered micropores, while the second step involved plasma etching to generate disordered nanopores. Micropores increase the optical path length, and nanopores significantly alter reflection through multiple refraction and transmission. Localized surface plasmon resonance (LSPR) Au generated [Fig. 24(e)] enhanced NIR absorption, reflectance, and transmittance, and the results showed near-complete absorption in the wavelength range of 220–1700 nm. The reflection was less than 5%, and the transmittance was less than 0.3%, as shown in Figs. 24(f) and 24(g). This work opens up new prospects for surface texturing and applications of black silicon.

The infrared absorption of black silicon can also be enhanced by coating with an NbN conformal film. Isakov *et al.*[68] fabricated black silicon by inductively coupled plasma etching ICP-RIE followed by the deposition of an NbN conformal film, which significantly increased the absorption of b-Si in a wide wavelength range (250–2500 nm). When the thickness of the NbN layer on b-Si was 15 nm, a high absorption of 99%–97% was achieved in the range of 1100–2500 nm, as shown in Fig. 25(a). The absorption

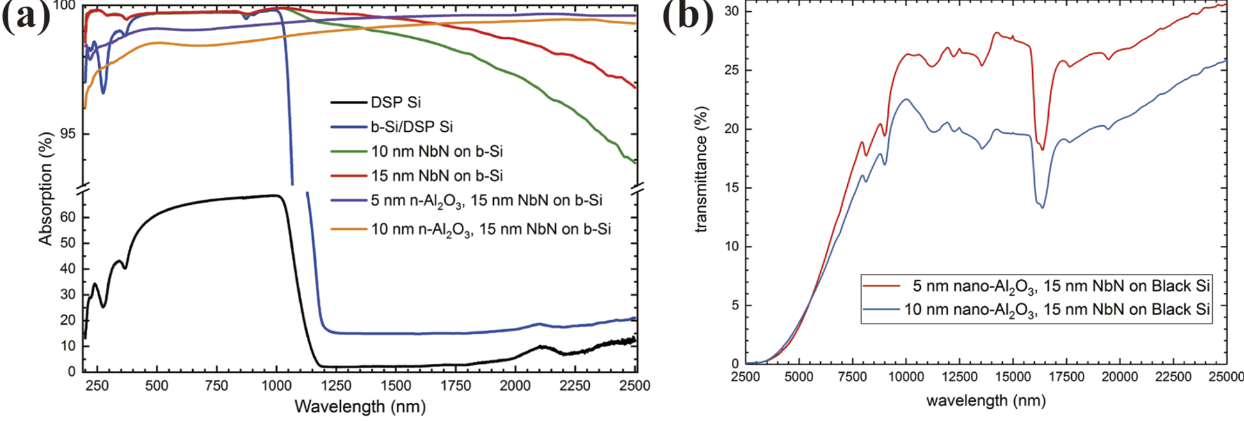

FIG. 25. (a) Absorption of 10 and 15 nm NbN on b-Si, 15 nm NbN on b-Si modified with 5 and 10 nm n-Al_2O_3, respectively, and DSP Si and b-Si/DSP Si. (b) Transmittance of black silicon coated with 15 nm NbN on b-Si modified with 5 and 10 nm n-Al_2O_3, respectively. Reprinted with permission from Isakov *et al.*, Nanotechnology **29**(33), 335303 (2018). Copyright 2018 IOP Publishing.

© Author(s) 2023

on double-sided polished silicon with NbN coating was only 50%, indicating that the high absorption is due to the synergistic combination of the microstructures of b-Si and NbN, rather than due to that of NbN alone. The broadband absorption properties of modified b-Si suggest that NbN-coated b-Si has promising application prospects in infrared microbolometers and infrared thermal imaging devices and deserves further study. In addition, the authors also added an alumina interlayer, which significantly increased the surface area of the NbN film, thereby further enhancing the absorption in the NIR region. In the wavelength region of 1300–2500 nm, the absorption was as high as 99.5%, and the transmittance was less than 1% at 4000 nm, as shown in Fig. 25(b). This approach could potentially enhance the infrared absorption of other developed structures and metamaterials. The technique offers significant improvement of the infrared absorption, including element doping, LSPR effect, and NbN film coating, compared with femtosecond laser-structured silicon nanostructures or chemically etched porous silicon structures.

Traditional methods to improve the infrared reflection of black silicon, such as Ag nanoparticles and oxide films, provide high absorption in the infrared wavelength range but have limited application in optoelectronics because they can only be used as passive components. In contrast, III–V nanowires provide another efficient light-trapping method. III–V materials can reach bandgaps as far as in the infrared region, allowing for stronger absorption of low-energy photons. More importantly, semiconductor nanowires can also serve as active parts in the device structure, offering fabrication possibilities that are not available with passive antireflection methods. Haggren *et al.*[69] first reported the application of a combination of black silicon substrates and III–V nanowires (NWs) in optoelectronic devices to achieve high broadband absorption. Black silicon was fabricated by ICP-RIE, and InAs NWs were grown on a p-type black silicon substrate at a low temperature of 280 °C. Figure 26 shows the (a) schematic and (b) cross-sectional SEM micrograph of this NW device after fabrication. The long-wave reflection decreased to about 15%, while the reflection below 1050 nm remained at 5%–7%, as shown in Fig. 26(c). The device exhibits perfect diode rectification behavior in the dark. Using black silicon as a growth platform for III–V materials, such as GaAs, InP, and InAs, can compensate for the disadvantage of black silicon's relatively high reflection in the infrared region. Furthermore, adjusting the nanowire density can reduce the reflection in different wavelength regions. This structure is very suitable for IR absorption and detection applications.

New process methods have also been proposed to innovate the original nano- and femtosecond lasers and thus improve the optical performance of textured silicon, such as laser cleaning technology, laser *in situ* deposition processing, and cooling laser processing substrates. Traditional HF cleaning is more harmful to the human body, while laser cleaning can not only effectively eliminate oxide deposition but also induce small-scale micro- and nanostructures on the silicon surface, thereby reducing the reflectivity of the material surface. Laser cleaning technology is based on the lower laser ablation threshold of contaminants compared with that of bulk materials, so contaminants can reach the threshold first and then be removed by vaporization, crushing, and stripping without damaging the substrate. In *in situ* deposition, nanoparticles are deposited on the edge of the etched microgrooves during laser irradiation, which increases the aspect ratio of the microgrooves and reduces the reflectivity of the material while reducing the complexity of traditional processing methods and simplifying the process steps. Cooling technology is a method that uses high-repetition rate laser irradiation to cool the material substrate and weaken the heat accumulation of femtosecond pulses on the material, thereby reducing the reflectivity of silicon. Based on these methods, high-performance broadband infrared response photodetectors have been fabricated.

Chen *et al.*[91] reported an efficient and economical method for the fabrication of multi-scale micro/nano-composite structures using the laser cleaning technology assisted by femtosecond laser ablation in the atmosphere. With a 625 μm p-type (100) silicon substrate, the average reflection of micro/nano-composite structured silicon is 2.06% in the infrared wavelength range of 0.3–2.5 μm and 4.98% in the broadband infrared wavelength range (2.5–16 μm), as shown in Fig. 27(a). This is the lowest reflection reported for laser processing technologies. At the same time, the laser cleaning

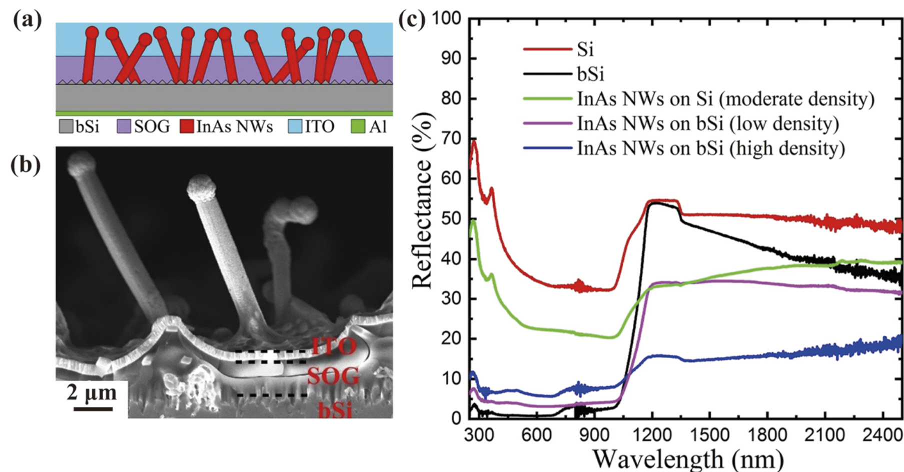

FIG. 26. (a) Schematic and (b) cross-sectional SEM micrograph of the NW device after fabrication. (c) Reflectance spectra of Si, black Si substrates, InAs NWs on Si with moderate density, and InAs NWs on black silicon with low and high density. Reprinted with permission from Haggren *et al.*, Sci. Rep. **8**(1), 6410 (2018). Copyright 2018 Springer Nature Limited.

© Author(s) 2023

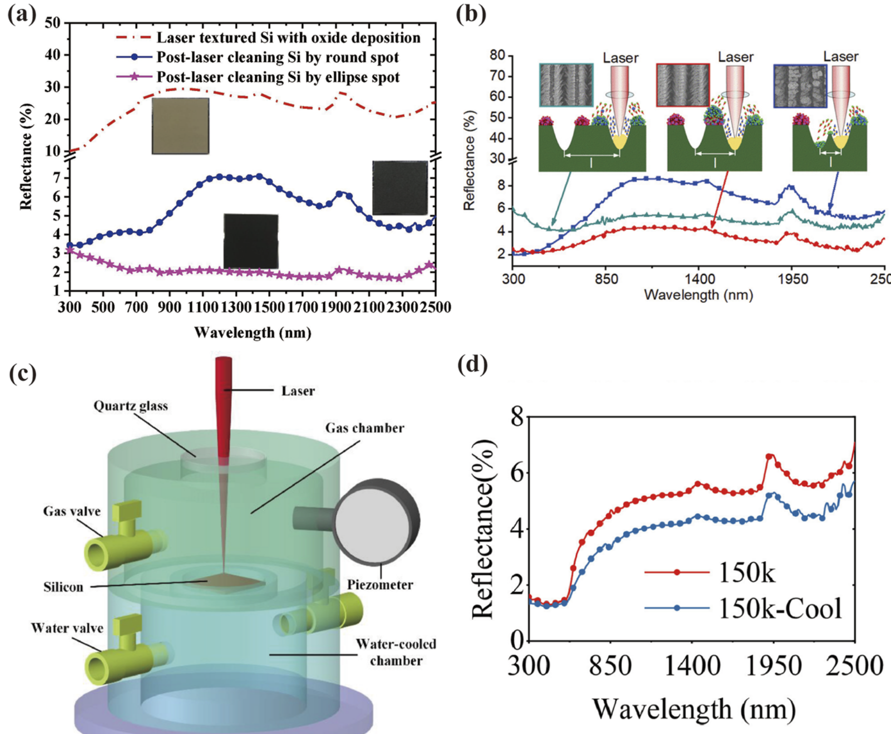

FIG. 27. (a) Reflectance spectra of laser-textured Si surfaces with and without laser cleaning by a round or elliptical light spot. Reprinted with permission from Chen *et al.*, Appl. Surf. Sci. **509**, 145182 (2020). Copyright 2020 Elsevier B.V. (b) Reflectance spectra and schematic of multiscale micro/nanostructures prepared via laser *in situ* deposition. Reprinted with permission from Chen *et al.*, ACS Appl. Mater. Interfaces **12**(43), 49265 (2020). Copyright 2020 American Chemical Society. (c) Schematic diagram of a water-cooled experimental device for laser processing. (d) Reflectance spectra of a Cu surface with different micro/nanostructures formed with and without water cooling at 150 K pulse repetition rates. Reprinted with permission from Chen *et al.*, Int. J. Heat Mass Transfer **164**, 120532 (2021). Copyright 2021 Elsevier Ltd.

efficiency can be increased by 4.8 times by replacing the circular with an elliptical light spot. This is beneficial for future applications of silicon-based infrared photodetectors. Chen *et al.*[92] also reported a new laser *in situ* deposition processing method. This method enables the synergistic fabrication of laser-ablated microstructures and the *in situ* deposition of high-porosity micro/nanostructures. The multi-scale micro/nano-structure is fabricated in one step, which simplifies the preparation process and achieves an overall improvement in the anti-reflection performance of the material surface. Figure 27(b) shows that the average reflectance of the Si surface reached 2.21% in the broadband (UV-NIR) region. Strong MIR absorption of the material surface over a wide wavelength range of 2.5–16 μm is achieved, and the average reflection of the silicon surface is only 5.28%. The multi-scale porous micro/nanostructures exhibited good broadband anti-reflection properties of the material surface, which is of great significance in optical and optoelectronic devices. However, the heat accumulated by subsequent laser pulses can increase the temperature of the material substrate and ultimately change the micro/nano-structure, affecting the anti-reflection performance. Thus, Chen *et al.*[93] proposed a strategy to fabricate antireflection structures by weakening the thermal accumulation of femtosecond pulses on materials to achieve a comprehensively improved antireflection performance in the UV-NIR region. The multiscale porosity of the surface structure was tuned by cooling the material substrate under laser irradiation with a high repetition rate, and the water-cooled experimental device for laser processing is shown in Fig. 27(c). Figure 27(d) shows that the average reflection of silicon was 3.50% when the pulse repetition rate was 150 kHz, and the silicon reflection decreased by 25.21%. Moreover, by increasing the pulse repetition rate, the processing speed is increased by three. This strategy provides a new and convenient way for the preparation of multi-scale porous micro/nanostructures of various structural absorption materials.

IV. ULTRAVIOLET DETECTION APPLICATIONS OF BLACK SILICON

To meet the detection requirements of silicon in the communication band, infrared detectors of black silicon have been intensively studied and further developed. The traditional silicon bandgap is 1.12 eV, which has good absorption for visible light below 1100 nm. For light at wavelengths above 1100 nm, high absorption can be achieved by element doping or other methods mentioned above, but for light of wavelengths of less than 400 nm, the existing technology has a low quantum efficiency and poor UV detection sensitivity. UV detection is prevalent in the production and life, in general, with a wide range of applications in astronomy, missile warning, pollution monitoring, and ultraviolet communication. At present, most UV detectors use wide bandgap semiconductor materials (GaN, SiC, etc.), but these materials have the problems of a small device scale and high cost. In contrast, large-scale and low-cost fabrication can be easier achieved with silicon-based UV detectors. Black silicon, as a silicon-based material, has excellent light absorption properties and advantages in achieving high quantum efficiency and sensitivity. Recently, the Brookhaven National Laboratory in the United States

© Author(s) 2023

and the Aalto University in Finland have developed a black silicon based ultraviolet optoelectronic device with an external quantum efficiency of 96% at 250–900 nm. Thus, the use of black silicon as a substrate for the detection of ultraviolet light is a very promising and challenging research topic.

Garin *et al.*[94] used an n-type high-resistance silicon wafer (>10 kΩ cm) as the substrate to fabricate black silicon by ICP-RIE. Figures 28(a) and 28(b) show the SEM images of nano-textured black-Si with the conelike and columnar-like morphology, respectively. A conformal Al_2O_3 film is deposited to form an induced junction for the fabrication of UV photodiodes, and the structure of these UV photodiodes is shown in the inset of Fig. 28(c). The EQE of photodiodes measured without external amplification was greater than 1. In particular, the EQE value reached 132% at 200 nm, as shown in Fig. 24(c). This high efficiency is due to the efficient use of multiple carrier generation by collisional ionization in nanostructures beyond the Shockley–Queisser limit. These photodiodes had a significant impact on the UV sensor industry.

Tsang *et al.*[95] reported vacuum ultraviolet (VUV) photodiodes and measured the spectral response under VUV irradiation at ambient and low temperatures. As the substrate, 675 μm FZ high-resistance silicon wafers (>10 kΩ cm) were used. The black silicon was fabricated by ICP-RIE at low temperatures, and the black silicon photodiodes were named Pin25sH (5×5 mm^2). Figures 28(d) and 28(e) show the photograph of the photodiodes. In combination with conformal alumina, the junction was induced, resulting in a quantum efficiency close to 1. The device has a dark current of 0.25 nA/cm^2 at room temperature and a responsivity of 0.2 A/W at 170 nm at room temperature in vacuum, as shown in Fig. 28(f). These results demonstrate new technologies for UV detection and pave the way for the development of high quantum-efficiency black silicon photomultipliers (b-SiPMs) required for the direct VUV photon detection in noble gas and liquid scintillation detectors. Both detectors use low-level doping and alumina deposition. Doping of black silicon with a low concentration of boron and phosphorus ions is beneficial for reducing the dark current and improving the device sensitivity. A conformal alumina antireflective film is used as a passivation layer to reduce the surface recombination loss and form an induced junction, which ensures an immediate collection of the photogenerated carriers. This novel structure shows that the formation of inductive nodes or self-built electric fields can effectively enhance the collection of photogenerated carriers and provide a way to realize UV detection.

V. SUMMARY AND OUTLOOK

With the rapid development of the semiconductor industry, silicon has become one of the most popular semiconductor materials due to its small size, wide range of applications, ease of integration, and long life. However, the bandgap of traditional silicon is only 1.12 eV, which severely limits its wavelength range for applications. At the same time, micro/nano-textured silicon overcomes the inherent wavelength limitation of the light absorption of silicon materials and has a high absorption in the near-infrared region. Therefore, achieving a high responsivity in optical communication bands, such as 1060, 1330, and 1550 nm, is one of the research goals of micro/nano-textured silicon-based photodetectors. Notably, black silicon substrates with excellent absorption properties have been fabricated, showing great potential in applications of infrared detection. Meanwhile, the manufactured high-performance black silicon based infrared photodetectors solve the shortcomings of commercial infrared detectors, such as high cost, high noise characteristics, and poor integration, with silicon-based electronic processes. They also improve the problems of traditional silicon-based photodetectors with a narrow spectral detection range, low efficiency, and low sensitivity. For black silicon that is promising to realize infrared detectors, two aspects can be optimized to enhance the performance. On the one hand, the structure of black silicon can be optimized by combining one or more methods, such as femto- and nanosecond laser, metal-assisted chemical etching, and ion reactive etching, or changing the preparation environment and process parameters, such as the temperature laser intensity, to make the microstructure of the black silicon surface more uniform. On the other hand, the physi-

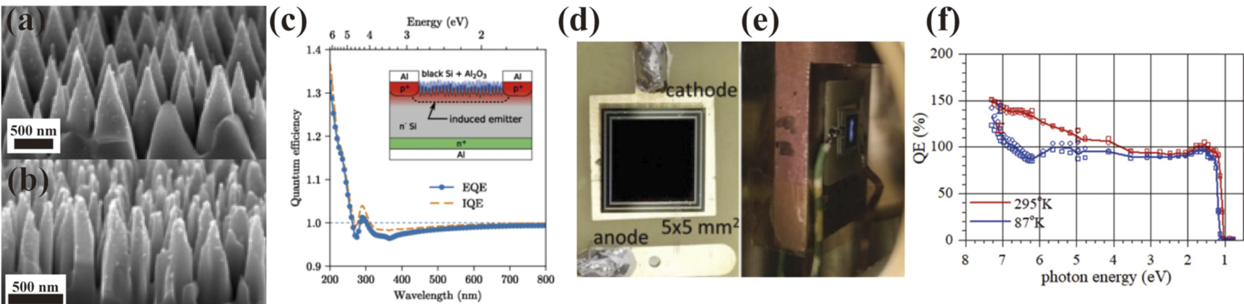

FIG. 28. (a) and (b) Bird's-eye view SEM image of black-Si nanotexture with cone- and columnar-like morphology. (c) External (blue circles) and internal (yellow dashed line) quantum efficiency of the induced-junction black-Si photodiode measured at zero bias. The inset schematically shows the structure of the device. Reprinted with permission from Garin *et al.*, Phys. Rev. Lett. **125**(11), 117702 (2020). Copyright 2020 American Physical Society.. (d) Black silicon photodiode (5×5 mm^2; model Pin25sH) mounted on a PC board. (e) A sample mounted on a copper cold finger illuminated at the center by VUV photons. (f) Measured quantum efficiency vs the incident photon energy of a b-Si photodiode (5×5 mm^2, Pin25sH) from 0.8 to 7.3 eV (1550–170 nm) at room temperature (red) and at 87 °K (blue). Open circles and squares indicate the data of two samples among two sets of results from the VUV and VIS/NIR measurements. The representative error bar for one sample is shown at the data points of 7.1 eV for both temperatures but in reverse color for clarity. Reprinted with permission from Tsang *et al.*, Opt. Express **28**(9), 13299 (2020). Copyright 2020 Optica Publishing Group.

© Author(s) 2023

cal properties of the material can be modified by combination with other process methods, such as element doping, LSPR effect, and heterojunction formation with other substances. For the infrared photodetectors based on the black silicon that have been manufactured, further optimization and improvement can be carried out in terms of passivation, self-driving, device size, and array. To enhance the UV absorption of black silicon, aluminum oxide can be used to form an induced junction and a self-built electric field. At the same time, black silicon based photodetectors can be fabricated using the novel detector structure and depositing a passivation layer to improve the photoresponse characteristics of the detector and obtain photodetectors with excellent response characteristics and high sensitivity. These photodetectors can be applied to night vision imaging, infrared pixel arrays, security monitoring, UV monitoring, UV communication, etc. There are already successful commercialization examples of black silicon photodetectors. For example, SIONYX has applied CMOS sensors based on black silicon for night vision devices, and ElFys provide a series of high-performance black silicon photodiodes for health monitoring and high-precision photometry. Although most black silicon based near-infrared and ultraviolet photodetectors are still in the laboratory research stage and cannot be commercialized, these photodetectors are very promising for applications of near-infrared and ultraviolet detection and promoting the development of the silicon-based detection technology.

ACKNOWLEDGMENTS

This work was supported by the National Natural Science Foundation of China (Grant No. 62101511), the Applied Basic Research Project of Shanxi Province (Grant No. 20210302124539), the Shanxi "1311 project" Key Subject Construction (Grant No. 1331 KSC), and Tan Kah Kee Innovation Laboratory (Grant No. RD2022020511).

AUTHOR DECLARATIONS

Conflict of Interest

The authors have no conflicts to disclose.

Author Contributions

Z.Z. and W.K. provided the whole concept. W.Y. and L.G. designed the structure of the review. Z.Z. wrote the hole review, J.J., G.R. and L.Z. drew figures, made tables and searched for the references. X.C. revised the manuscript before it was submitted. All authors participated in modifying the manuscript.

Zhou Zhao: Data curation (lead); Investigation (lead); Visualization (lead); Writing – original draft (lead); Writing – review & editing (lead). **Zengxing Zhang**: Conceptualization (equal); Supervision (equal); Writing – review & editing (equal). **Junmin Jing**: Formal analysis (supporting); Investigation (supporting). **Rui Gao**: Data curation (supporting); Investigation (supporting). **Zhiwei Liao**: Data curation (supporting); Investigation (supporting). **Wenjun Zhang**: Data curation (supporting); Investigation (supporting). **Guohua Liu**: Conceptualization (supporting); Supervision (supporting). **Yonghua Wang**: Conceptualization (supporting); Supervision (supporting). **Kaiying Wang**: Conceptualization (equal); Supervision (supporting); Writing – review & editing (supporting). **Chenyang Xue**: Supervision (equal); Writing – review & editing (equal).

DATA AVAILABILITY

Data sharing is not applicable to this article as no new data were created or analyzed in this study.

REFERENCES

[1] H. Jansen, M. de Boer, R. Legtenberg, and M. Elwenspoek, J. Micromech. Microeng. **5**, 115 (1995).

[2] T.-H. Her, R. J. Finlay, C. Wu, S. Deliwala, and E. Mazur, Appl. Phys. Lett. **73**(12), 1673 (1998).

[3] S. Sarkar, A. A. Elsayed, Y. M. Sabry, F. Marty, J. Drévillon, X. Liu, Z. Liang, E. Richalot, P. Basset, E. Nefzaoui, and T. Bourouina, Adv. Photonics Res. **3**, 2200223 (2022).

[4] M. A. Juntunen, J. Heinonen, H. S. Laine, V. Vähänissi, P. Repo, A. Vaskuri, and H. Savin, Proc. SPIE **10249**, 102490I (2017).

[5] Z. Fan, D. Cui, Z. Zhang, Z. Zhao, H. Chen, Y. Fan, P. Li, Z. Zhang, C. Xue, and S. Yan, Nanomaterials **11**(1), 41 (2020).

[6] E. Özkol, P. Procel, Y. Zhao, L. Mazzarella, R. Medlin, P. Šutta, O. Isabella, and M. Zeman, Phys. Status Solidi RRL **14**(1), 1900087 (2019).

[7] C.-H. Hsu, S.-M. Liu, W.-Y. Wu, Y.-S. Cho, P.-H. Huang, C.-J. Huang, S.-Y. Lien, and W.-Z. Zhu, Arabian J. Chem. **13**(11), 8239 (2020).

[8] M. A. Juntunen, J. Heinonen, V. Vähänissi, P. Repo, D. Valluru, and H. Savin, Nat. Photonics **10**(12), 777 (2016).

[9] G. Mi, J. Lv, L. Que, Y. Zhang, Y. Zhou, and Z. Liu, Nanoscale Res. Lett. **16**(1), 38 (2021).

[10] X. Jin, Q. Wu, S. Huang, G. Deng, J. Yao, H. Huang, P. Zhao, and J. Xu, Opt. Mater. **113**, 110874 (2021).

[11] C. Wen, W. Chen, Y. P. Chen, K. J. Liu, X. H. Li, S. F. Hu, and Y. J. Yang, Mater. Res. Bull. **93**, 238 (2017).

[12] F. Atteia, J. Le Rouzo, L. Denaix, D. Duché, G. Berginc, J. J. Simon, and L. Escoubas, Mater. Res. Bull. **131**, 110973 (2020).

[13] J. Heinonen, C. Modanese, A. Haarahiltunen, H. Kettunen, M. Rossi, J. Jaatinen, and M. A. Juntunen, Nucl. Instrum. Methods Phys. Res., Sect. A **977**, 164294 (2020).

[14] Y. Nishijima, H. Nishijima, and S. Juodkazis, Sol. Energy Mater. Sol. Cells **217**, 110706 (2020).

[15] Y. Xia, B. Liu, J. Liu, Z. Shen, and C. Li, Sol. Energy **85**(7), 1574 (2011).

[16] Y. Xia, B. Liu, S. Zhong, and C. Li, J. Electron Spectrosc. Relat. Phenom. **184**(11–12), 589 (2012).

[17] H. D. Omar, M. R. Hashim, and M. Z. Pakhuruddin, Opt. Laser Technol. **136**, 106765 (2021).

[18] C. Wu, C. H. Crouch, L. Zhao, J. E. Carey, R. Younkin, J. A. Levinson, E. Mazur, R. M. Farrell, P. Gothoskar, and A. Karger, Appl. Phys. Lett. **78**(13), 1850 (2001).

[19] R. Younkin, J. E. Carey, E. Mazur, J. A. Levinson, and C. M. Friend, J. Appl. Phys. **93**(5), 2626 (2003).

[20] A. Y. Vorobyev and C. Guo, Appl. Surf. Sci. **257**(16), 7291 (2011).

[21] B. Franta, D. Pastor, H. H. Gandhi, P. H. Rekemeyer, S. Gradečak, M. J. Aziz, and E. Mazur, J. Appl. Phys. **118**(22), 225303 (2015).

[22] S. Zhong, B. Liu, Y. Xia, J. Liu, J. Liu, Z. Shen, Z. Xu, and C. Li, Sol. Energy Mater. Sol. Cells **108**, 200 (2013).

[23] J. W. M. Lim, S. Huang, L. Xu, Y. Y. Lim, Y. X. Loh, C. S. Chan, K. Bazaka, I. Levchenko, and S. Xu, Sol. Energy **171**, 841 (2018).

[24] J. S. Yoo, I. O. Parm, U. Gangopadhyay, K. Kim, S. K. Dhungel, D. Mangalaraj, and J. Yi, Sol. Energy Mater. Sol. Cells **90**(18–19), 3085 (2006).

[25] Y. Bi, X. Su, S. Zou, Y. Xin, Z. Dai, J. Huang, X. Wang, and L. Zhang, Thin Solid Films **521**, 176 (2012).

© Author(s) 2023

[26]Z. Zhang, T. Martinsen, G. Liu, M. Tayyib, D. Cui, M. J. de Boer, F. Karlsen, H. Jakobsen, C. Xue, and K. Wang, Adv. Opt. Mater. **8**(19), 2000668 (2020).
[27]D. Dimova-Malinovska, M. Sendova-Vassileva, N. Tzenov, and M. Kamenova, Thin Solid Films **297**(1–2), 9 (1997).
[28]X. Li and P. W. Bohn, Appl. Phys. Lett. **77**(16), 2572 (2000).
[29]S. Koynov, M. S. Brandt, and M. Stutzmann, Appl. Phys. Lett. **88**(20), 203107 (2006).
[30]H. M. Branz, V. E. Yost, S. Ward, K. M. Jones, B. To, and P. Stradins, Appl. Phys. Lett. **94**(23), 231121 (2009).
[31]N. A. Md. Noor, S. K. Mohamad, S. S. Hamil, M. Devarajan, and M. Z. Pakhuruddin, Mater. Sci. Semicond. Process. **91**, 167 (2019).
[32]J. Lv, T. Zhang, P. Zhang, Y. Zhao, and S. Li, Nanoscale Res. Lett. **13**(1), 110 (2018).
[33]C. Li, J.-H. Zhao, Y. Yang, Q.-D. Chen, Z.-G. Chen, and H.-B. Sun, IEEE Sens. J. **21**(22), 25695 (2021).
[34]K. N. Nguyen, P. Basset, F. Marty, Y. Leprince-Wang, and T. Bourouina, J. Appl. Phys. **113**(19), 194903 (2013).
[35]Q. Tan, F. Lu, C. Xue, W. Zhang, L. Lin, and J. Xiong, Sens. Actuators, A **295**, 560 (2019).
[36]J. Y. H. Chai, B. T. Wong, and S. Juodkazis, Mater. Today Energy **18**, 100539 (2020).
[37]T. H. Fung, T. P. Pasanen, Y. Zhang, A. Soeriyadi, V. Vähänissi, G. Scardera, D. Payne, H. Savin, and M. Abbott, Sol. Energy Mater. Sol. Cells **210**, 110480 (2020).
[38]C. Huo, J. Wang, H. Fu, X. Li, Y. Yang, H. Wang, A. Mateen, G. Farid, and K. Q. Peng, Adv. Funct. Mater. **30**(52), 2005744 (2020).
[39]M. Y. Arafat, M. A. Islam, A. W. B. Mahmood, F. Abdullah, M. Nur-E-Alam, T. S. Kiong, and N. Amin, Sustainability **13**(19), 10766 (2021).
[40]S. Huang, G. Deng, X. Jin, Y. Lu, G. Song, H. Huang, P. Zhao, C. Zhang, J. Yao, Q. Wu, and J. Xu, Opt. Mater. **110**, 110474 (2020).
[41]B. F. Andresen, M. U. Pralle, G. F. Fulop, J. E. Carey, H. Homayoon, P. R. Norton, S. Alie, J. Sickler, X. Li, J. Jiang, D. Miller, C. Palsule, and J. McKee, Proc. SPIE **7660**, 218 (2010).
[42]J. Heinonen, A. Haarahiltunen, M. D. Serue, V. Vähänissi, T. P. Pasanen, H. I. Savin, L. Werner, and M. A. Juntunen, Proc. SPIE **11276**, 112760G (2020).
[43]K. Wang, S. Liu, J. Li, S. Wu, J. Xia, J. Chen, C. Tian, Y. Liu, and Z. Zhong, J. Mater. Sci.: Mater. Electron. **32**(9), 11503 (2021).
[44]S. Singh, A. Sarkar, D. K. Goswami, and S. K. Ray, ACS Appl. Energy Mater. **4**(4), 4090 (2021).
[45]A. Sarkar, S. Mukherjee, A. K. Das, and S. K. Ray, Nanotechnology **30**(48), 485202 (2019).
[46]H. Zhong, N. Ilyas, Y. Song, W. Li, and Y. Jiang, Nanoscale Res. Lett. **13**(1), 316 (2018).
[47]Z. Zheng, Q. Luo, K. Xu, Z. Liu, and K. Zhu, Opto-Electron. Eng. **48**(5), 200364 (2021).
[48]S. Paulus, P. Mc Kearney, F. Völklein, and S. Kontermann, AIP Adv. **11**(7), 075014 (2021).
[49]X. Zhan, H. Xu, C. Li, H. Zang, C. Liu, J. Zhao, and H. Sun, Opt. Lett. **42**(3), 510 (2017).
[50]Y. Su, X. Zhan, H. Zang, Y. Fu, A. Li, H. Xu, S.-L. Chin, and P. Polynkin, Appl. Phys. B **124**(11), 223 (2018).
[51]X.-Y. Yu, J.-H. Zhao, C.-H. Li, Q.-D. Chen, and H.-B. Sun, IEEE Trans. Nanotechnol. **16**(3), 502 (2017).
[52]C.-H. Li, J.-H. Zhao, Q.-D. Chen, J. Feng, and H.-B. Sun, Opt. Lett. **43**(8), 1710 (2018).
[53]C.-H. Li, X.-P. Wang, J.-H. Zhao, D.-Z. Zhang, X.-Y. Yu, X.-B. Li, J. Feng, Q.-D. Chen, S.-P. Ruan, and H.-B. Sun, IEEE Sens. J. **18**(9), 3595 (2018).
[54]S. Huang, Q. Wu, Z. Jia, X. Jin, X. Fu, H. Huang, X. Zhang, J. Yao, and J. Xu, Adv. Opt. Mater. **8**(7), 1901808 (2020).
[55]J.-H. Zhao, Z.-H. Lv, C.-H. Li, X.-Y. Yu, and X.-B. Li, IEEE Sens. J. **17**, 1000 (2017).
[56]Y. Yang, J.-H. Zhao, C. Li, Q.-D. Chen, Z.-G. Chen, and H.-B. Sun, Opt. Lett. **46**(13), 3300 (2021).
[57]Y. Su, D. Yao, S. Wang, X. Zhan, and H. Xu, Opt. Laser Technol. **123**, 105913 (2020).
[58]Z. Jia, Q. Wu, X. Jin, S. Huang, J. Li, M. Yang, H. Huang, J. Yao, and J. Xu, Opt. Express **28**(4), 5239 (2020).
[59]F. Hu, X.-Y. Dai, Z.-Q. Zhou, X.-Y. Kong, S.-L. Sun, R.-J. Zhang, S.-Y. Wang, M. Lu, and J. Sun, Opt. Express **27**(3), 3161 (2019).
[60]F. Hu, L. Wu, X. Dai, S. Li, M. Lu, and J. Sun, Photonics Res. **9**(7), 1324 (2021).
[61]S. Uddin, M. R. Hashim, and M. Z. Pakhuruddin, Mater. Sci. Semicond. Process. **133**, 105932 (2021).
[62]M. Franz, R. Junghans, P. Schmitt, A. Szeghalmi, and S. E. Schulz, Beilstein J. Nanotechnol. **11**, 1439 (2020).
[63]K. Chen, T. P. Pasanen, V. Vahanissi, and H. Savin, IEEE J. Photovoltaics **9**(4), 974 (2019).
[64]Y. Ryu, S. Hwang, J. Lee, and T. Kim, J. Nanosci. Nanotechnol. **19**(4), 2202 (2019).
[65]P. Cheng, H. Wang, B. Müller, J. Müller, D. Wang, and P. Schaaf, ACS Appl. Mater. Interfaces **13**(1), 1818 (2021).
[66]Y. Song, T. Liu, S. Liu, J. Huang, J. Li, C. Tian, T. Yu, Y. He, Y. Liu, and Z. Zhong, J. Mater. Sci.: Mater. Electron. **31**(6), 4696 (2020).
[67]Z. Zhang, Y. Wang, P. A. Stensby Hansen, K. Du, K. R. Gustavsen, G. Liu, F. Karlsen, O. Nilsen, C. Xue, and K. Wang, Nano Energy **65**, 103992 (2019).
[68]K. Isakov, A. P. Perros, A. Shah, and H. Lipsanen, Nanotechnology **29**(33), 335303 (2018).
[69]T. Haggren, V. Khayrudinov, V. Dhaka, H. Jiang, A. Shah, M. Kim, and H. Lipsanen, Sci. Rep. **8**(1), 6410 (2018).
[70]D. Hu, Y. Wang, Y. Wang, W. Huan, X. Dong, and J. Yin, Mater. Lett. **312**, 131653 (2022).
[71]H. Yao, X. Guo, A. Bao, H. Mao, Y. Ma, and X. Li, Chin. Phys. B **31**(3), 038501 (2022).
[72]Y. Sun, L. Xie, Z. Ma, Z. Qian, J. Liao, S. Hussain, H. Liu, H. Qiu, J. Wu, and Z. Hu, Nanomaterials **12**(3), 371 (2022).
[73]Q. Zhu, P. Ye, Y. Tang, X. Zhu, Z. Cheng, J. Xu, and M. Xu, Nanotechnology **33**(11), 115202 (2021).
[74]C. Wang, F. Zhao, Z. Zhou, X. Li, S. He, M. Zhang, D. Zhang, and L. Zhang, J. Alloys Compd. **905**, 164245 (2022).
[75]H. Karakachian, P. Rosenzweig, T. T. N. Nguyen, B. Matta, A. A. Zakharov, R. Yakimova, T. Balasubramanian, Z. Mamiyev, C. Tegenkamp, C. M. Polley, and U. Starke, Adv. Funct. Mater. **32**(18), 2109839 (2022).
[76]C. G. Kang, S. J. Kim, B.-H. Kim, Y. S. Kim, J. M. Park, H. S. Kim, J. H. Ha, H. Choi, M. Chae, K. Oh, B. Lee, and N.-H. Lee, J. Korean Phys. Soc. **77**(9), 754 (2020).
[77]Q. Wu, G. Cen, Y. Liu, Z. Ji, and W. Mai, Phys. Lett. A **412**, 127586 (2021).
[78]X. Chen, C. Yang, H. Sun, S. Ning, H. Zhou, H. Zhang, S. Wang, G. Feng, and S. Zhou, Laser Phys. Lett. **16**(7), 076201 (2019).
[79]Y. Tang and J. Chen, Superlattices Microstruct. **150**, 106803 (2021).
[80]M. Shiraishi, T. Enoki, K. Kobayashi, S. Yasunaga, Y. Ajiki, and T. Kan, Jpn. J. Appl. Phys. **60**(7), 076501 (2021).
[81]H. Lin, A. Jiang, S. Xing, L. Li, W. Cheng, J. Li, W. Miao, X. Zhou, and L. Tian, Nanomaterials **12**(6), 910 (2022).
[82]L. Lv, J. Yu, M. Hu, S. Yin, F. Zhuge, Y. Ma, and T. Zhai, Nanoscale **13**(14), 6713 (2021).
[83]W. Yang, J. Chen, Y. Zhang, Y. Zhang, J. H. He, and X. Fang, Adv. Funct. Mater. **29**(18), 1808182 (2019).
[84]J. Heinonen, T. P. Pasanen, V. Vahanissi, M. A. Juntunen, and H. Savin, IEEE Trans. Electron Devices **67**(4), 1645 (2020).
[85]J.-H. Zhao, C.-H. Li, X.-B. Li, Q.-D. Chen, Z.-G. Chen, and H.-B. Sun, IEEE Trans. Electron Devices **65**(11), 4905 (2018).
[86]L. Wang, Z.-F. Ren, K.-Y. Wang, S.-J. He, and L.-B. Luo, Mater. Res. Express **4**(4), 045022 (2017).
[87]K. Kim, S. Yoon, M. Seo, S. Lee, H. Cho, M. Meyyappan, and C.-K. Baek, Nat. Electron. **2**(12), 572 (2019).
[88]T. Zhang, W. Ahmad, B. Liu, Y. Xuan, X. Ying, Z. Liu, Y. Li, Z. Chen, and S. Li, Mater. Lett. **196**, 16 (2017).
[89]T. Zhang, B. Liu, W. Ahmad, Y. Xuan, X. Ying, Z. Liu, Z. Chen, and S. Li, Nanoscale Res. Lett. **12**(1), 522 (2017).

© Author(s) 2023

[90]K. Gorgulu, M. Yilmaz, K. Topalli, and A. K. Okyay, J. Opt. **19**(6), 065101 (2017).
[91]T. Chen, W. Wang, T. Tao, A. Pan, and X. Mei, Appl. Surf. Sci. **509**, 145182 (2020).
[92]T. Chen, W. Wang, T. Tao, A. Pan, and X. Mei, ACS Appl. Mater. Interfaces **12**(43), 49265 (2020).
[93]T. Chen, W. Wang, T. Tao, Y. Zhang, and X. Mei, Int. J. Heat Mass Transfer **164**, 120532 (2021).
[94]M. Garin, J. Heinonen, L. Werner, T. P. Pasanen, V. Vähänissi, A. Haarahiltunen, M. A. Juntunen, and H. Savin, Phys. Rev. Lett. **125**(11), 117702 (2020).
[95]T. Tsang, A. Bolotnikov, A. Haarahiltunen, and J. Heinonen, Opt. Express **28**(9), 13299 (2020).

© Author(s) 2023